Applied Geochemistry 201 (2026) 106766

Contents lists available at ScienceDirect

Applied Geochemistry

journal homepage: www.elsevier.com/locate/apgeochem

Contrasting behaviour in geogenic degassing along an active segment of the East Anatolian fault zone (Türkiye)

G. Yüce [a,b], W. D'Alessandro [b,*], C.C. Fu [c], F. Italiano [d,e], M. İçhedef [f], H. Elmacı [g], B. Kürkcüoğlu [a], B. Kahraman [a], A. Demirtaş [a], L.H. Lin [h], D. Yasin [i], Ş. Gürboğa [j], A. Özdemir [a], L. Li Vigni [b,k], M. Tantillo [b], H. Akıllı [g], A. Çiçek [g], L. Taşkıran [g], M. Toklu [l], S. Över [m], T. Kılıç [n]

[a] Hacettepe University, Department of Geological Engineering, Beytepe, Ankara, Türkiye
[b] Istituto Nazionale di Geofisica e Vulcanologia (INGV), Palermo, Italy
[c] Academia Sinica, Institute of Earth Sciences, Taipei, Taiwan
[d] Istituto Nazionale di Oceanografia e di Geofisica Sperimentale (OGS), Trieste, Italy
[e] Athanor-Geotech srls, via GregorioVII 396, Rome, 00165, Italy
[f] Ege University, Institute of Nuclear Sciences, Bornova-Izmir, 35100, Türkiye
[g] General Directorate of Mineral Research and Exploration, Çankaya, Ankara, Türkiye
[h] Department of Geosciences, National Taiwan University, Taipei, Taiwan
[i] Eskişehir Osmangazi University, Department of Geological Engineering, Eskişehir, Türkiye
[j] İstanbul Technical University, Faculty of Mines, Department of Geological Engineering, Ayazağa, İstanbul, Türkiye
[k] University of Palermo, DiSTeM, Palermo, Italy
[l] State Hydraulic Works, Dept. of Groundwater, Ankara, Türkiye
[m] Iskenderun Technical University, Civil Engineering Department, Hatay, Türkiye
[n] Ministry of Interior, Disaster and Emergency Management Authority (AFAD), Ankara, Türkiye

ARTICLE INFO

Editorial handling by Daniele L. Pinti

Keywords:
Osmaniye fault
Tectonic degassing
He isotopes
Soil CO_2 fluxes
^{222}Rn

ABSTRACT

Seismically active areas have long been recognised as hotspots of geogenic degassing. The present study investigated the Osmaniye Fault which belongs to the East Anatolian Fault Zone (EAFZ). Although EAFZ has been recently (February 2023) hit by the destructive Kahramanmaraş earthquake, the studied segment was not involved and is still accumulating stress. Three areas along this structure were selected with gas samples collected and analysed for their chemical and isotope compositions. Extensive CO_2-flux measurements were performed together with some soil gas Rn measurements in two of the areas. The three areas were characterised by very different degassing behaviour both in term of chemical and isotope composition and in term of CO_2 output.

In the first (area A), signs of anomalous degassing are visible with several thousands of m^2 showing stunted or absent vegetation, strong alteration of the soils and extensive surface deposits of sulfur and sulfates efflorescences. The CO_2-flux measurements yielded a wide range of values (1.3-57,200 g m^{-2} day^{-1}). Soil Rn activity was generally very low (0.1-1.7 kBq m^{-3}). Soil gas chemistry indicates a mixing between atmospheric air and a CO_2-rich deep geogenic end-member ($\delta^{13}C \sim 0‰$). Helium isotope composition indicates a high mantle contribution ($R/R_A \sim 6$).

Area B, on the contrary, shows very low soil flux values (0.4-57 g m^{-2} day^{-1}), almost all compatible with organic activity in the soil, low Rn activity (0.3-5.6 kBq m^{-3}) and strongly negative $\delta^{13}C$–CO_2 values (<-21.7‰).

In area C, geogenic degassing can be recognised only as gas bubbling in a hyperalkaline (pH ~ 12) spring. The gases comprise predominantly CH_4 of likely abiotic origin. The absence of deep-derived CO_2 suggests consumption either by carbonate precipitation or through reactions with H_2 produced during serpentinization processes occurring in the ultramafic rocks of the area. Deep origin of at least part of the gases is supported by the substantial contribution of mantle He ($R/R_A \sim 3$).

Estimation of the total CO_2 output of area A gave a value of about 20,000 t a^{-1}. Such output value, comparable with a quiescent volcanic system, further underscores the important contribution of geogenic degassing along

* Corresponding author.
E-mail address: walter.dalessandro@ingv.it (W. D'Alessandro).

https://doi.org/10.1016/j.apgeochem.2026.106766
Received 22 September 2025; Received in revised form 28 January 2026; Accepted 6 March 2026
Available online 8 March 2026

active tectonic structures to the natural carbon cycle. Periodic and/or continuous monitoring of gaseous emissions in the same area would be useful to obtain possible precursory signals.

1. Introduction

Seismically active regions are considered areas of anomalous geogenic degassing. Numerous studies have focused on quantifying the release of geogenic CO_2 into the atmosphere across different geological environments (e.g., Kerrick, 2001; Burton et al., 2013; Fischer et al., 2019). In recent decades, the tectonic carbon degassing has been recognised as a significant contributor to the global carbon cycle (e.g., Chiodini et al., 2011; Yüce et al., 2017; Daskalopoulou et al., 2019; D'Alessandro et al., 2020; Randazzo et al., 2021; Li Vigni et al., 2022, 2025). The relationship between tectonically active regions and deeply-derived fluid migration has been well-documented since long time (Barnes et al., 1978). The spatial distribution and amount of geogenic fluids released into the atmosphere are strongly influenced by regional normal and transcurrent faulting, as well as the lengths of continental rifts (Brune et al., 2017; Tamburello et al., 2018). Indeed, active deep fault systems, sometimes characterized by enhanced porosity and permeability, are the preferential pathways for the escape of advective fluids, which carry gases such as CO_2 and He from the deep crust or mantle to the atmosphere (e.g., Irwin and Barnes, 1980; Faulkner et al., 2010; Tamburello et al., 2018). Additionally, these geogenic fluids may actively contribute to the generation of deep earthquakes (e.g., Du et al., 2006; Chiodini et al., 2020; Caracausi et al., 2022). Natural gases observed along fault lines in seismically active regions may provide crucial insights into tectonic processes and subsurface dynamics, being natural indicators of fault activity and stress accumulation (Toutain and Baubron, 1999; Yang et al., 2005; Fu et al., 2009, 2017).

Additionally, regions of plate collision, like Southern Türkiye, are often areas in which ophiolitic sequences outcrop abundantly (Dilek and Thy, 1998, 2009). Ophiolites generally comprise in their sequence ultramafic rocks where low temperature continental serpentinization processes may produce abundant molecular hydrogen (Leong et al., 2023). In the presence of adequate catalytic elements (Etiope and Ionescu, 2015), it may produce also abiotic methane reacting with oxidized carbon species (CO_2, CO, HCO_3^- etc.) through Fischer-Tropsch-like reactions (Etiope and Sherwood Lollar, 2013). Such reactions have been evidenced in the Turkish ophiolitic massifs of Kızıldağ (Yüce et al., 2014; D'Alessandro et al., 2018) and Tekirova (Etiope et al., 2011).

Türkiye is located between the Eurasian, African, and Arabian plates, undergoing deformation controlled by numerous structures, primarily the North Anatolian and East Anatolian fault zones (Şengör and Yılmaz, 1981; Barka and Kadinsky-Cade, 1988; Reilinger et al., 2006; Emre et al., 2018) (Fig. 1a). The East Anatolian Fault Zone (EAFZ) is one of the most seismically active regions in Türkiye and the broader Middle East. On February 6, 2023, a destructive earthquake with a moment magnitude of 7.8 struck the Kahramanmaraş province in south-eastern Türkiye, occurring along the EAFZ (Fig. 1b). The left-lateral strike-slip earthquake was an unpredictable seismic hazard in terms of its magnitude and destructive capacity for the tectonic setting of the region, which is influenced by the interactions of three major plates (Anatolian, Arabian, and African). The recent earthquake involved multiple segments, specifically the Pazarcık, Karasu, and Erkenek segments in its southern part (Ş;engör et al., 1985; Karabacak, 2007; Karabacak et al., 2012; Duman and Emre, 2013). A number of studies have been published just after the earthquake, dealing with the different aspect of earth sciences (Akinci et al., 2025; Barbot et al., 2023; Gökçeoğlu, 2023; Jia et al., 2023; Karabacak et al., 2023; Kocaman, 2023; Melgar et al., 2023; Reitman et al., 2023; Rosakis et al., 2023; Akar, 2024; Gürboğa et al., 2024; Meng et al., 2024; Akıncı et al., 2025; Hu et al., 2025; Meghraoui et al., 2025; Sharma and Biswas, 2025). The total surface rupture length has been estimated to be 400 km by Gökçeoğlu (2023), 345 km by Reitman et al. (2023), 270 km by Karabacak et al. (2023) and in 264 km by Gürboğa et al. (2024).

The geological history of the EAFZ indicates that this fault system has a long record of large earthquakes, both in historical and instrumental periods. This ongoing seismic activity raises significant concerns for the safety and preparedness of communities in the region.

The 2023 Kahramanmaraş earthquake was a major geological event

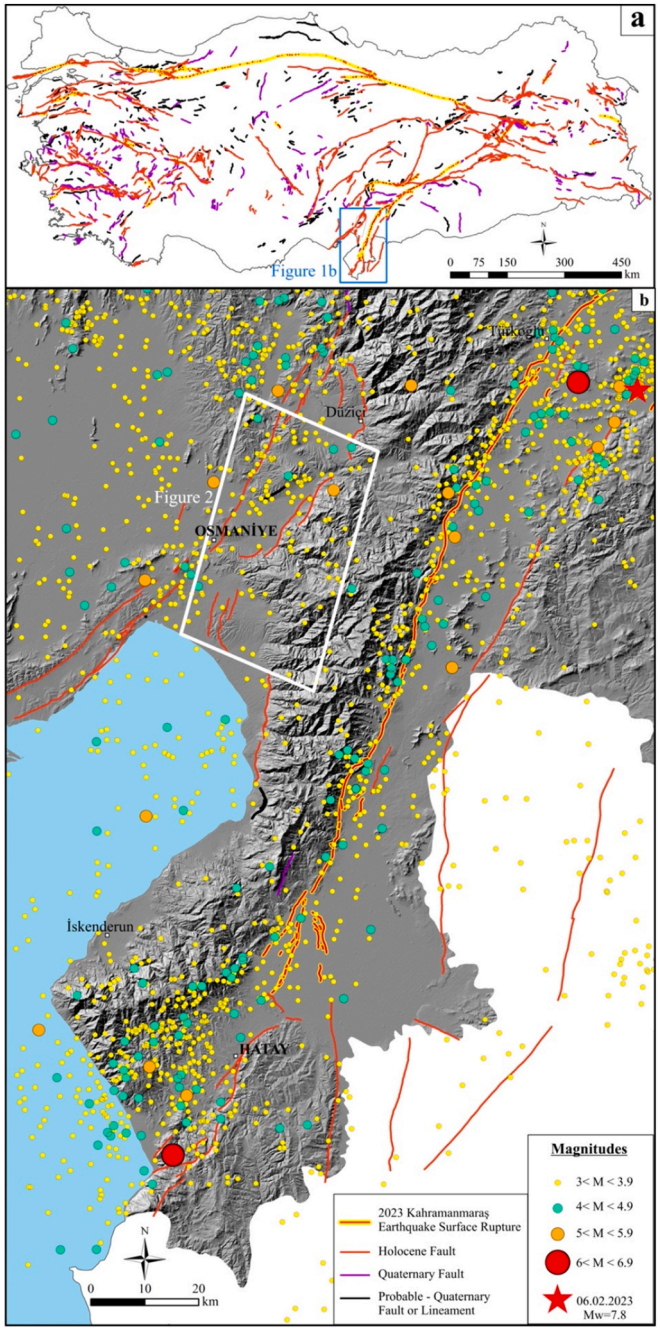

Fig. 1. a) Active tectonic map of Türkiye (Emre et al., 2018); b) Tectonic map of the region around the study area (Emre et al., 2018; Kürçer et al., 2023; Elmacı et al., 2024) and epicentral distribution of the earthquakes bigger than magnitude 3 between 1900 and 2025 compiled from AFAD catalogue.

that not only caused widespread destruction but also provided a unique opportunity to investigate fundamental tectonic processes, including stress transfer between interacting fault segments, rupture segmentation, and fault-controlled fluid migration. Understanding these processes is essential because they directly control the spatial and temporal evolution of seismic hazard, including the likelihood of stress loading on neighboring fault segments, the potential for triggered seismicity, and the modification of subsurface permeability that governs fluid migration. In tectonically active regions such as southeastern Türkiye, where multiple major fault systems interact, such knowledge is critical for improving earthquake forecasting models, hazard assessment, and resilience-oriented mitigation strategies, particularly when integrated with geological, geophysical, and geochemical observations.

The TUBITAK project 123Y301, based on previous studies of fluid's geochemistry in the area (Italiano et al., 2013; Yüce et al., 2014, 2017; D'Alessandro et al., 2018), is intended to investigate the geochemical processes affecting fluids circulating along the EAFZ, with a special focus on areas in which tectonic stress is still accumulating. In this framework, the present study focusses on the geogenic degassing of an active fault system close to the town of Osmaniye, in the southeast part of Türkiye. The study comprises: i) the chemical and isotope analyses of the gases released in three different areas along the Osmaniye segment of EAFZ, investigating the origin of the different species, ii) the measurement of the CO_2 gas flux from the soil for the quantification of the CO_2 output of the area and iii) the assessment of the potential use of the site for continuous and/or periodic gas monitoring as a precursor of the fault activity in the area.

2. Geological and tectonic settings

2.1. Geological setting

The geodynamic history of the Eastern Mediterranean from the Late Cretaceous to the Miocene is characterized by the collision of the African–Arabian plates with the Eurasian plate that caused the migration of the Anatolian block west-southwest along the Eastern Mediterranean Arc. This is accommodated by two significant transform fault systems: The North Anatolian Fault Zone (NAFZ) and the East Anatolian Fault Zone (EAFZ) (Şengör and Yılmaz 1981; Hempton, 1987; Barka and Reilinger, 1997). The collision connecting south-eastern Türkiye to the

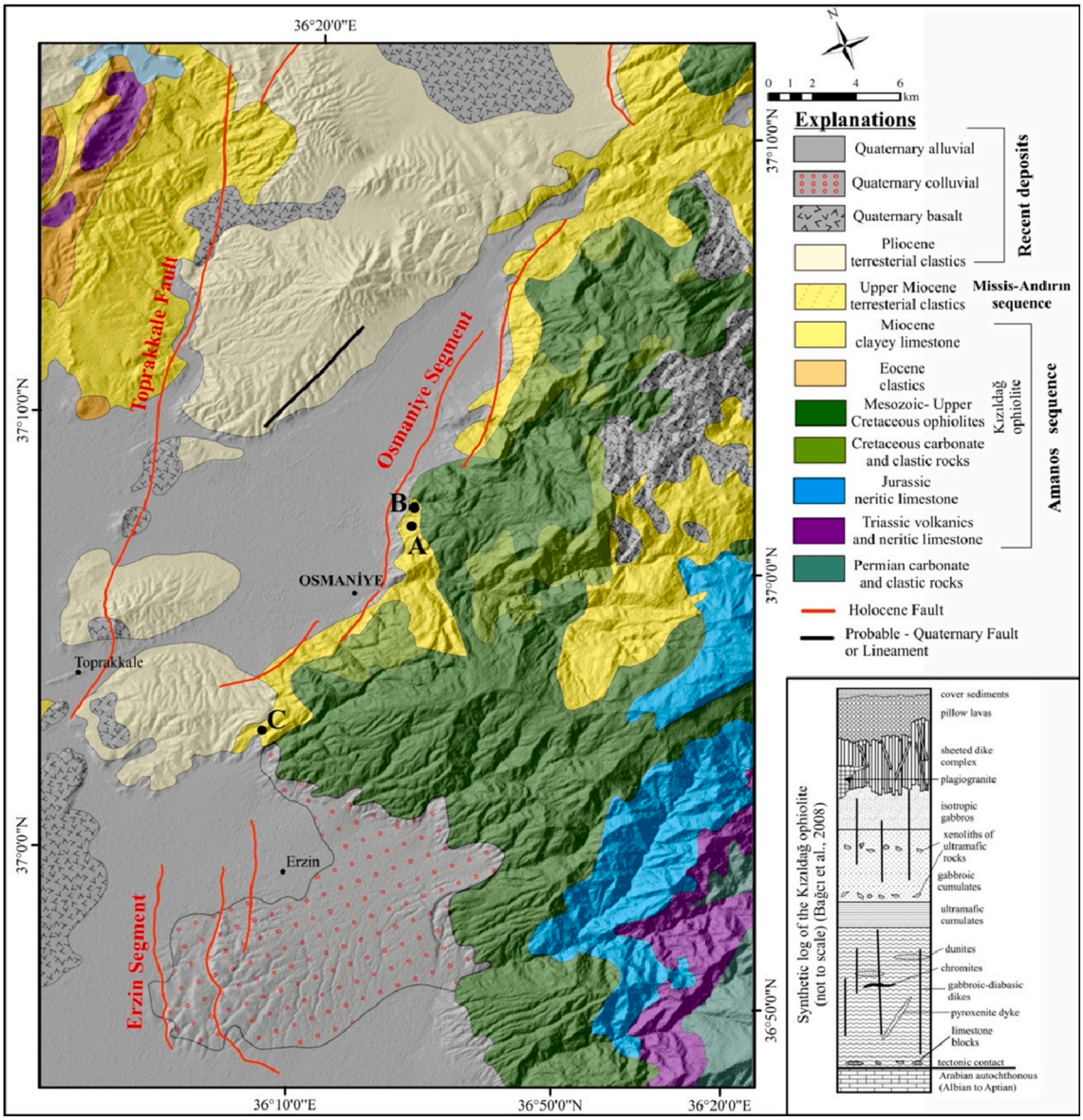

Fig. 2. Geological map of the study area (based on Sümengen, 2014). The position of the three studied areas (A, B and C) is shown on the map.

Eastern Mediterranean basin runs through the Misis-Andırın, and Amanos ranges (Fig. 1). Osmaniye is also located on the collision area comprising a composite geological setting, mainly Mesozoic–Early Tertiary carbonate and terrigenous sedimentary rocks, along with basic–ultrabasic ophiolite-related units, and tectonic features, mega scale left-lateral EAFZ and many active faults.

Geological setting of the Osmaniye region is composed of three groups of sequences; the Amanos, Misis-Andırın sequences and the Pliocene-Quaternary cover units that unconformably lie on two older sequences (Sümengen, 2014; Beyazpirinç and Usta, 2018). The Amanos sequence ranges in age from the Early Ordovician to the Middle Miocene with quartzite and quartzitic sandstones interbedded with siltstones and shales. Due to the widespread tectonic movements in the late Campanian-early Maastrichtian the ophiolitic mélange (Kızıldağ ophiolite) was emplaced (Fig. 2). The Kızıldağ ophiolite is one of the most complete ophiolitic sequences in the world with a thickness of 8500 m (Bağcı et al., 2005; Dilek and Thy, 2009; Tanırlı and Rızaoğlu, 2016; Şimşek et al., 2023).

The Misis-Andırın succession is located on the Amanos succession with a tectonic contact. The sequence is mainly composed of the Andırın limestone and Andırın mélange comprising a strongly mixed unit including blocks of different ages and types in a fluvial matrix (Fig. 2).

These two sequences have been covered by the Pliocene and Quaternary volcanics and recent alluvial deposits as basin fill (Fig. 2). The Adana Basin is an important sedimentary basin formed by extensional tectonics and hosts thick sequences of clastic and carbonate sediments, around 6 km thick (Willams et al. 1995; Yetiş et al., 1995; Burton-Ferguson et al., 2005). Thus, Quaternary volcanics called the Delihalil Basalt is a tholeiitic plateau basalt that emerges around Yumurtalık, Ceyhan, Osmaniye, and Haruniye from the main outcrop centre at Delihalil Tepe. Titaniferous augite, augite and olivine micrograins, and plagioclase microliths make up the matrix, whilst the basaltic lavas are often intergranular porphyritic in texture and composed of plagioclase, and olivine phenocrysts (Bilgin and Ercan, 1981). Arger et al. (2000) reported in this area K–Ar ages spanning from 0.61 ± 0.10 to 2.25 ± 0.78 Ma and thus attributable to the Quaternary period.

2.2. Tectonic setting and seismicity of the area

The tectonic evolution of the Osmaniye region is dominated by the convergence of the Anatolian, Arabian, and African plates. A series of phases are described in literature related to Tethys evolution (Robertson et al., 2004). A Late Permian–Triassic rifting of the Southern Tethys, followed by a Mesozoic carbonate platform formation by passive margin subsidence. During the latest Cretaceous, subduction/accretion an ophiolite sequence was emplaced along the northern margin by obduction upon the Arabian margin. Ophiolitic and arc-type units in the volcano-sedimentary unit, slices and blocks in the melange are examples of oceanic crust that formed above a N-dipping subduction zone in relation to the partial closure of the Tethys. Northern and southern margins of the Southern Tethys underwent renewed, mainly carbonate, deposition on a restored passive margin in Palaeocene – Early Eocene. Later on, northward subduction resumes the accretion of the Misis-Andırın range in the Late Eocene-Oligocene. The earliest Miocene period (Aquitanian) marked the end of melange genesis. Neritic carbonate and then deeper water clastic deposits covered the old accretionary prism. Then, Mid-Late Miocene is the time when the convergence resumes, with the emplacement of a turbidite basin and suture tightening. Lastly, along the EAFZ and its westward prolongation as fault strands, dominantly left-lateral strike-slip allowed for the continuation of regional N–S convergence (Şengör et al., 1985; Dewey et al., 1986; Reilinger et al., 2006). The tectonic structure of the area is a result of the left lateral strike-slip movement of the EAFZ that has persisted to recent and enlarged into a broad fault area (Şaroğlu, 1985; Koçyiğit et al., 2001; Şengör et al., 2003). The area has a number of fault zones and segments that are active and have the potential to create destructive events as was seen in the 2023 earthquakes. There are three active fault systems around the town of Osmaniye (Fig. 1b and 2) which are Toprakkale fault, Erzin and Osmaniye segments of the EAFZ (Emre et al., 2018). The Osmaniye Segment is 24 km long with N45°E striking, 65° NW dipping. It is a normal fault with Holocene activity and can probably produce Mw: 6.68 earthquakes (Wells and Coppersmith, 1994).

According to the seismotectonic map of Türkiye, focal mechanism solutions along the fault segments indicate a normal faulting dominant mechanism. Based on the catalogue of the Disaster and Emergency Management Authority (AFAD), 303 events with magnitude $3<M<4$, 24 with magnitude $4<M<5$ and 3 earthquakes with magnitude $5<M<6$ took place after occurrence of the first shock.

3. Methods

3.1. Selection of the study area

The area of Osmaniye has been included in the ongoing TUBITAK project 123Y301 because in June 2013 the groundwater sample collected at a local spring, analysed for its dissolved He isotope composition, gave a R_C/R_A value of 5.55 indicating a strong mantle contribution (D'Alessandro et al., 2018 and Table S1). During the first campaign of the present project in May 2024, the same spring was found dry. Local inhabitants claimed that the spring had dried out as a consequence of the February 2023 earthquakes. Looking up to find alternative groundwater sampling sites we found at a distance of few hundred meters two zones with visible signs of anomalous degassing. These included several thousands of m^2 of land showing stunted or absent vegetation, strong alteration of the soils and extensive surface deposits of sulfur and sulfate efflorescences. There are also indications of excavation, potentially for the extraction of sulfur or alum. Pictures of all these features can be found in the supplementary material. At one of these zones gas was bubbling in a rainwater pond. The analysis of the collected gas sample confirmed the presence of a deep degassing component (sample A34 May 2024 – Fig. 3a and Table S1). Therefore, we decided to study in detail this area (A) in the following sampling campaign in September 2024. For comparison, we extended our measurements to other two areas (B and C) along the same tectonic system (Figs. 2 and 3). Area B, about 1 km north of area A, was chosen to compare an area with no signs of degassing, easily accessible to make two parallel traverses intersecting the Osmaniye fault trace, while area C was included, although further away (about 10 km south-west) because previous studies (D'Alessandro et al., 2018) indicated a significant mantle contribution for helium in the bubbling gases of the hyperalkaline spring.

3.2. Sampling and analytical methods

In May and September 2024 and in June 2025, three sampling campaigns were carried out. Sixteen gas samples have been collected in the study area: 5 bubbling gases and 11 soil gases. Samples have been collected in borosilicate (Pyrex) glass vessels with two vacuum stopcocks for He isotope analysis and in Exetainer© Labco vials for chemical and for carbon isotopic compositions of CO_2, CH_4 and C_2H_6 or hydrogen isotopic compositions of CH_4.

Bubbling gases were collected filling the sampler with the water in which the gas was bubbling and placing an inverted funnel connected to the sampler above the gas bubbling. As soon as the gas had displaced the water inside, the sampler was closed. Soil gases were collected by inserting a pipe (3 mm inner diameter) in the soil at about 50 cm depth and driving the gas by a syringe and a 3-way valve to the gas sampler.

The analyses of the gas samples were carried out at the laboratories of Istituto Nazionale di Geofisica e Vulcanologia of Palermo (INGV-Pa). The concentrations of He, H_2, H_2S, O_2, N_2, CO_2, CH_4, and C_2 and C_3 alkanes of the samples were determined by an Agilent 7890B gas

Fig. 3. Detailed maps of the three studied areas A, B and C. The positions of all gas sampling sites are indicated with a red dot while all CO_2-flux measurement points are displayed as white dots.

chromatograph with Ar as carrier, equipped with a 4-m Carbosieve S II and PoraPlot–U columns. A Thermal Conductivity Detector has been used to measure the concentrations of He, O_2, N_2, and CO_2 and a Flame Ionization Detector for CH_4 and C_2 and C_3 alkanes. The analytical errors have been estimated in less than 5 % for He, H_2, H_2S, and C_2 and C_3 alkanes and 3 % for O_2, N_2, CH_4, and CO_2.

Carbon isotopes of CO_2, CH_4 and C_2H_6 and hydrogen isotopes of CH_4 have been measured at INGV-Pa using a Thermo TRACE GC interfaced to a Delta Plus XP gas source mass spectrometer, equipped with a Thermo GC/C III (for carbon) and with GC/TC peripherals (for hydrogen) and expressed as δ ‰ notation ($\delta = (R_{sample}/R_{standard} - 1) * 1000$ where R is the isotope ratio). The $^{13}C/^{12}C$ ratios are reported as $\delta^{13}C–CO_2$, $\delta^{13}C–CH_4$ and $\delta^{13}C–C_2H_6$ ‰ values (precision ±0.15 ‰) with respect to the V-PDB standard while $^{2}H/^{1}H$ ratios are reported here as $\delta^{2}H–CH_4$ values (precision ±2.0 ‰) with respect to the V-SMOW standard.

The abundance and isotope composition of He, and the $^{4}He/^{20}Ne$ ratios, have been determined either at INGV-Pa or at the Department of Geosciences, National Taiwan University (NTU) by separately admitting He and Ne into a Split Flight Tube Noble Gas Mass Spectrometer (Helix SFT). Helium isotope compositions are given as R/R_A, where R is the ($^{3}He/^{4}He$) ratio of the sample and R_A is the atmospheric ($^{3}He/^{4}He$) ratio ($R_A = 1.386 \times 10^{-6}$). The analytical errors were generally <1 %. Samples analysed at INGV-Pa for He isotopes were also analysed for Ar isotopes ($^{40}Ar/^{36}Ar$ and $^{38}Ar/^{36}Ar$) with a Static Vacuum Mass Spectrometer (Argus VI).

Radon in the soil was measured with a RAD7 electronic radon detector that aspirates gas through a probe inserted into the soil at 50 to 70 cm depth. Measurements of soil gas radon was made at 5-min intervals over 4 cycles. Simultaneous measurements of CO_2 and O_2 concentrations were made with a GASLAB PRO multi-gas data logger.

Carbon dioxide flux has been measured with the accumulation chamber method (Chiodini et al., 1998) at 176 sites with a portable soil fluxmeter (WEST Systems, Italy). Flux values have been determined at each site from the rate of CO_2 concentration increase in the chamber and are expressed in the current work in grams per square meter per day ($g \times m^{-2} \times d^{-1}$) after conversion from volumetric to mass concentrations considering the measured atmospheric pressure and temperature values. The portable soil fluxmeter is equipped with a Licor LI820 IR spectrometer characterized by a reproducibility better than 20 % in the measuring range 10 - 20,000 $g \times m^{-2} \times d^{-1}$. The used accumulation chamber has an area of 0.031 m^2 and a volume of 0.0028 m^3. Care has been taken to follow the recommendations for flux measurements as proposed by Lewicki et al. (2005). Flux measurements were made only in two of the selected areas (A and B). No flux measurement has been made in area C because of limited time during the sampling campaign, but considering that the gas bubbling in the spring has very low concentrations in CO_2, typical of hyperalkaline springs, the presence of deep CO_2 degassing in this area is very unlikely. Measurements have been made on the 20th and 21st of September for area A and on the 24th of September for area B. Weather was stable during the whole period with no sharp variations in atmospheric pressure nor strong winds.

The CO_2 flux data were elaborated by both statistical and geostatistical tools. The GSA method (Chiodini et al., 1998), based on Sinclair's partitioning method (Sinclair, 1974), was used to characterize the CO_2 flux. This method allows the partitioning of polymodal statistical distribution into individual populations and the definition of populations statistical parameters and relative proportions. Because the gas flux data resulted a combination of log-normal distributed populations, the computed mean and standard deviation of the partitioned populations refer to the logarithm of CO_2 flux values, the mean of the CO_2 flux and the 95% confidence interval of the mean were thus estimated by the Sichel's t-estimator (David, 1977).

The map of the CO_2 fluxes was drawn using the sequential Gaussian simulations (sGs method; Cardellini et al., 2003). The sGs method consists of the production of numerous equiprobable realizations of the spatial distribution of the CO_2 flux by using the sgsim algorithm of the

GSLIB software library (Deutsch and Journel, 1998) according to the variogram model of the normal score of the CO_2 flux derived from the experimental variogram. In the present study, 100 equiprobable realizations were computed for the area using a computational grid of 2 × 2 m. The CO_2 flux map is then reported as map of the "expected'' values at any cell (E-type estimates), obtained through a pointwise linear average of all the realizations (Deutsch and Journel, 1998). The results of the sGs were also used to estimate the total CO_2 output summing the products of simulated value at each grid cell by the cell surface. The mean and the standard deviation of the 100 simulated values of total CO_2 output, computed for the 100 realizations, were assumed to be the characteristic values of the CO_2 output of its uncertainty for the area.

4. Results

Chemical and isotope compositions and geographic coordinates of the gas samples are reported in Table S1 (supplementary material). Carbon dioxide (up to 990,400 μmol mol^{-1}) is the principal component in all but one of the soil gas samples of area A, while nitrogen and oxygen (up to 782,000 and 202,200 μmol mol^{-1} respectively) prevail in the soil gases of area B, indicating a dominant air component (Fig. 4a). Methane (up to 953,000 μmol mol^{-1}) is the main component of the gas bubbling in the hyperalkaline spring of area C (Fig. 4b). Significant CH_4 concentrations (up to 1400 μmol mol^{-1}) are generally found also in the gases of area A, while in area B it shows no detectable concentration (<1 μmol mol^{-1}). Helium ranges from 7 to 107 μmol mol^{-1} with the highest values measured in area C. Hydrogen ranges from <3 to 3080 μmol mol^{-1} with values often in the order of hundreds of μmol mol^{-1} in both areas A and C and less than the detection limit in area B. Finally, H_2S and C_3H_8 are systematically <10 μmol mol^{-1}, while C_2H_6 is found only in area C (1940 to 3380 μmol mol^{-1}).

The isotopic composition of $\delta^{13}C$–CO_2 ranges from −0.3 to 1.5 ‰ in area A and from −23.3 to −21.7 ‰ in area B. No data on $\delta^{13}C$–CO_2 is available for area C. Methane shows $\delta^{13}C$–CH_4 values between −26.9 and −26.0 ‰ in area A and between −8.5 and −7.9 ‰ in area C, while $\delta^{2}H$–CH_4 values could be measured only in area C (−157 to −132 ‰). On two samples of area C also $\delta^{13}C$–C_2H_6 values (−21.9 and −21.2 ‰) have been measured.

Helium isotope analyses gave R/R_A values from 4.85 to 5.34, with $^4He/^{20}Ne$ ratios between 1.84 and 36.7 at area A, while in area C they ranged respectively from 2.45 to 3.14 and from 1.26 to 158. Argon isotopic ratios were in the range 296.4 – 304.0 ($^{40}Ar/^{36}Ar$) and 0.1866 – 0.1870 ($^{38}Ar/^{36}Ar$) for both area A and C. Neither He nor Ar isotope values were obtained for area B.

Areas A and B exhibit notable differences in soil gas concentrations. Soil gas radon activity concentrations were between 21.6 and 5603.3 Bq m^{-3}. The mean and median concentrations for radon calculated were 1623.5 and 873.7 Bq m^{-3}, respectively. In Area A, radon levels ranged from 21.6 to 1733.3 Bq m^{-3}, whereas in Area B, they varied between 349.0 and 5603.3 Bq m^{-3}. The temperature recorded by the RAD7 device and the multigas data logger were generally consistent, with values ranging between approximately 27 °C and 46 °C.

Soil CO_2 fluxes measured in the areas A and B range from 0.4 to 57,200 g m^{-2} d^{-1} and can be considered as the overlapping of three log-normal populations in area A and two log-normal populations in area B (Fig. 5). Statistical parameters are reported in Table 1. All flux data and geographic coordinates are reported in Table S1 (Supplementary Material).

5. Discussion

5.1. Characterization of the main sources of the gases in the three areas

The three investigated areas show very different chemical and isotope gas composition suggesting distinct sources for the gases.

5.1.1. Atmospheric gases

The constituent most apparently identified is related to the atmospheric air (N_2, O_2, and Ar). The composition of the soil gases of area A and B fall along a mixing line between the atmospheric air composition and a CO_2-rich deep degassing component (Fig. 6a). The atmospheric component, excluding sample contamination during sampling, can be added to the gas mixture either by meteoric recharge, which can deliver atmospheric gases up to great depths within the hydrologic circuit, or by diffusion within the soil in a much shallower environment. These two processes can generally be discriminated by the N_2/O_2 ratio. The atmospheric component deriving from diffusion within the soil maintains almost the same molar ratio of atmospheric air (N_2/O_2 = 3.7). The soil gases of both area A and B show ratios close to air (3.8 – 5.9), while samples with less than about 10,000 μmol mol^{-1} N_2 display slightly higher values (up to 8.5). Instead, the gases bubbling in the hyperalkaline spring of area C show much higher N_2/O_2 ratios (36 – 570), pointing to oxygen consumption through redox reactions within the hydrologic circuit (Fig. 6b). The strongly reducing conditions in the hyperalkaline spring water (Yüce et al., 2014) support the oxygen consumption hypothesis.

The few available argon isotope data indicate no other source (crustal or mantle) than atmospheric air for this gas.

5.1.2. Carbon dioxide

Regarding the second end-member in the mixing line between atmospheric and deep origin gases, it has a CO_2-dominant composition (CO_2 > 95%vol – Fig. 6a). The carbon isotope composition of CO_2 in the less air-contaminated samples is −0.3 ‰ (Fig. 7), indicating a likely

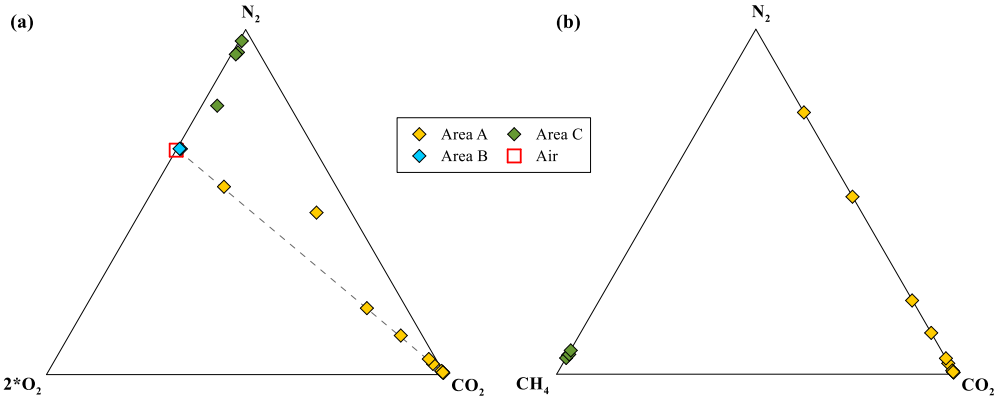

Fig. 4. Chemical composition of the sampled gases. (a) O_2–CO_2–N_2 and (b) CH_4–CO_2–N_2 ternary diagrams. The atmospheric air (N_2/O_2 = 3.7) composition is also plotted.

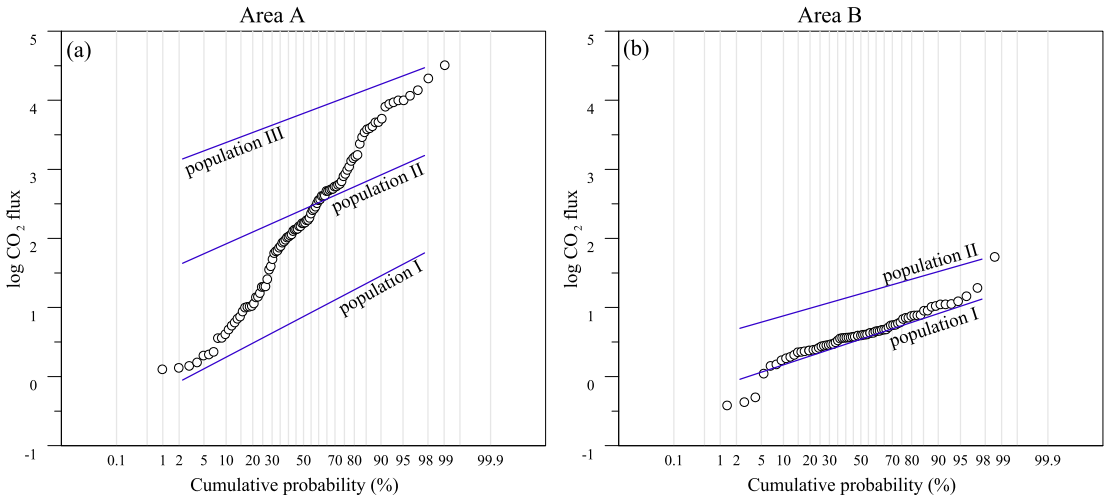

Fig. 5. Probability plot of the CO_2 fluxes from (a) area A and (b) area B. The blue lines represent the partitioned populations.

Table 1
Statistical parameters of CO_2 flux populations.

Area A					
Populations	Mean CO_2 flux	σ	Proportion	Area	CO_2 output
	g m^{-2} d^{-1}		*%*	*m^2*	*t d^{-1}*
I	11.9	0.46	30.7	35,900	0.13
II	389	0.39	50.5		6.98
III	8513	0.33	18.8		58.1
					65.2
Area B					
Populations	Mean CO_2 flux	σ	Proportion	Area	CO_2 output
	g m^{-2} d^{-1}		*%*	*m^2*	*t d^{-1}*
I	4.45	0.29	90.4	101,700	0.40
II	19.1	0.25	9.6		0.17
					0.58

origin from decarbonation of marine limestones (Sano and Marty, 1995). The two samples of area B, instead, show a strongly negative (<−21.7 ‰) $\delta^{13}C–CO_2$ (Fig. 7), indicating an almost purely organic source (Sano and Marty, 1995). The samples of area A with lower CO_2 contents do not align along a mixing line between the deep geogenic source and the shallow organic one. This most probably depends on the fact that samples were collected in areas devoid of vegetation with strongly altered soil with scarce organic content. On the contrary, the samples align along a fractionation line pointing towards slightly more positive values (Fig. 7). This could be due to diffusion kinetic fractionation owing to the concentration gradient between the soil CO_2 and the atmospheric air that permeates the soil (Camarda et al., 2007).

Finally, the samples collected in area C have very low CO_2 contents (<800 μmol mol^{-1}) which is a typical feature of hyperalkaline springs. The very high pH of the water induces a complete dissolution of CO_2 and its transformation in HCO_3^- and CO_3^{2-} ions. The small CO_2 quantities, sometimes measured, are not in equilibrium with the water and probably derive from shallow sources (atmosphere, organic activity) due to mixing with shallow aquifers.

5.1.3. *Light alkanes*

The only area in which light alkanes were always below detection limit was area B. on the contrary, at area C, CH_4 represents more than 90 %vol of the gases and ethane has a concentration of about 3000 μmol mol^{-1}, while propane was below detection limit (<10 μmol mol^{-1}). As previously highlighted by D'Alessandro et al. (2018), many pieces of evidence point to an abiotic origin of these alkanes. The authors (D'Alessandro et al., 2018) support their conclusions with: i) the strongly positive isotope composition of both carbon and hydrogen of methane; ii) the more negative value of $\delta^{13}C–C_2H_6$ with respect to $\delta^{13}C–CH_4$, and iii) the strongly correlated ($r^2 > 0.99$) Shultz-Flory distribution (decreasing concentration with increasing carbon number – Etiope and Sherwood Lollar, 2013) of the alkanes. The close geographic connection with the Kızıldağ ophiolite outcrops and the bubbling of the collected samples in a hyperalkaline spring supports the origin of these gases from Fisher-Tropsch-like reactions, which are favoured by the probable presence of catalysing elements, such as

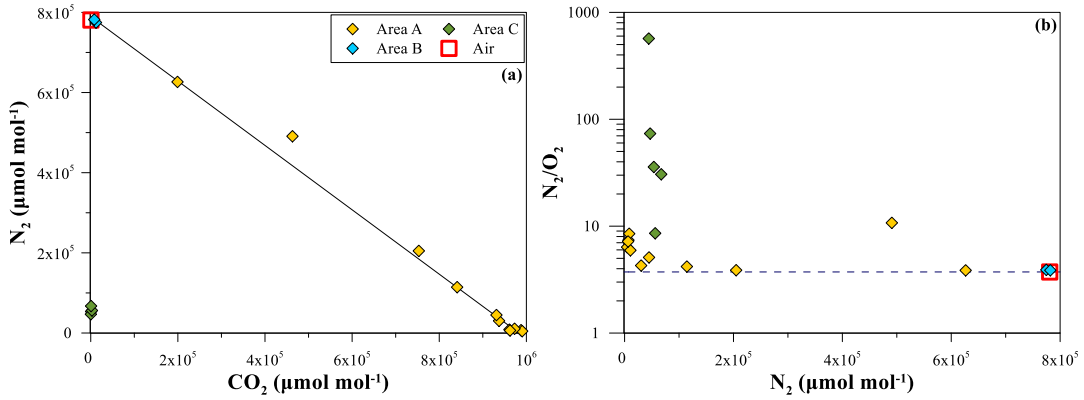

Fig. 6. a) CO_2 vs. N_2 binary plot and b) N_2/O_2 vs. N_2 binary plot. The atmospheric air (N_2/O_2 = 3.7) composition is also plotted.

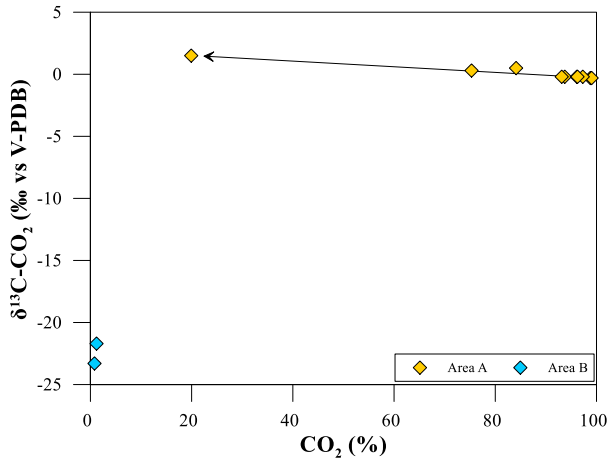

Fig. 7. CO_2 vs. $\delta^{13}C$–CO_2 (‰ vs. V-PDB) binary plot. The black arrow represents the kinetic fractionation of $\delta^{13}C$–CO_2 due to diffusion through the soil in area A (Camarda et al., 2007).

Ruthenium (Etiope and Ionescu, 2015). This element is particularly enriched in chromite accumulations within ophiolitic sequences (Etiope and Ionescu, 2015), which are also found in the Kızıldağ massif (Dilek and Thy, 2009). These hypotheses suggest that the origin of active economic methane occurrence close to study area may be ascribable to an abiogenic source related to serpentinization processes in the Kızıldağ ophiolite sequences.

As reported in the result section, alkane concentrations in area A are much lower, with CH_4 concentrations within the typical range of hydrothermal systems (Chiodini, 2009). Also the carbon isotope composition of CH_4 (around −26.5 ‰) is close to the range of values generally measured for geothermal CH_4 (Fiebig et al., 2013; Milkov and Etiope, 2018). Such values have been generally attributed either to abiotic reactions within a geothermal reservoir (Daskalopoulou et al. 2018) or to thermal degradation of organic matter (Fiebig et al., 2019). We did not have the possibility to measure other parameters, such as $C_1/(C_2+C_3)$ alkane ratio or δ^2H–CH_4, that would have been helpful in better constraining the origin of the alkanes in area A gases. However, the first hypothesis can be supported by the active abiogenic serpentinization processes in the Amanos Mountain ranges close to the study area (Yüce et al., 2014).

Although no anomalous temperature has been measured at the surface, and the measured concentrations and C-isotope composition of CH_4 may be explained by other processes, the presence of a hot water reservoir at depth cannot definitely be ruled out.

5.1.4. Hydrogen

The presence of hydrogen has long been evidenced in gases collected along active faults and its variations have sometimes been related to seismic activity (Sugisaki et al., 1983; Sato et al., 1986; Hirose et al., 2011). Previous studies demonstrated that concentrations in soil gases range from below detection limit up to several % with the highest concentration mainly linked to seismic structures related to historical earthquakes (Sugisaki et al., 1983). Spike-like hydrogen anomalies may also be due to the increase in permeability along the seismic structure as a consequence of stress built-up releasing accumulated hydrogen of various origin (Sato et al., 1986; Zhou et al., 2021). Sources of hydrogen may be multiple, although organic processes, radiolysis and the mantle have been considered to be negligible in such environment. Sugisaki and coworkers (Sugisaki et al., 1983) considered the reaction of water with freshly exposed surfaces of silicate rocks due to the tectonic stress as one of the main sources within active faults. Another source, suggested by Sato and coworkers (Sato et al., 1986) is the oxidation of ferrous iron in olivines and pyroxenes in mafic rocks yielding magnetite and gaseous H_2. Similarly, ultramafic rocks alteration (serpentinization, carbonation, etc) produces this gas even at temperatures as low as 30 °C (Neubeck et al., 2014). Low temperature production may also be suggested by δ^2H–H_2 values around 700‰ similar to many continental serpentinization areas, like for example the nearby Kizildag massif (D'Alessandro et al., 2018). Even altered ultramafic rocks, if still rich in ferrous iron, can be source of H_2 through iron oxidation reactions.

Although H_2 production may be obtained at low temperature, higher temperature (200-350 °C – Mayhew et al., 2013) may increase reaction kinetic and therefore hydrothermal systems release generally H_2-rich gases.

In the study area, H_2 has been found in concentrations up to few thousands of μmol mol^{-1}. Being the area characterised by the presence of active tectonic structures, by outcropping basaltic flows and ophiolite sequences, and by increased geothermal gradients (Bilim et al., 2017), all the above suggested processes may be the source of this gas. Furthermore, being hydrogen highly reactive, concentrations above 100 μmol mol^{-1} measured in soils have been considered as derived from steadily active processes (Sugisaki et al., 1983). Some of them, like water-rock interactions sustained by serpentinization reactions, hydrothermalism and active stress accumulation along the fault, may be considered active in the studied areas.

5.1.5. Helium

Helium isotope composition is a strong discriminant between crustal and mantle sources whose R/R_A values are very different with the former around 0.01 (Ballentine and Burnard, 2002) and the latter, around 8, considering a MORB-like mantle (Ozima and Podosek, 2002). Atmospheric gases have an intermediate value of 1 for R/R_A but their contribution can be easily discriminated by measuring the $^4He/^{20}Ne$ ratio, which is very different (0.318) from that of the other two main sources (>1000). Indeed, when the atmospheric contamination is not too high, like in the gases collected for this study (measured $^4He/^{20}Ne$ ratios between 1.26 and 36.7), the isotope ratio of the sample can be recalculated eliminating the atmospheric component following the method of Sano and Wakita (1985). The corrected values (R_C/R_A) range from 2.94 to 3.20 for area C and from 5.38 to 5.95 for area A, indicating a strong mantle contribution corresponding to 35 - 40% and 70 - 75% respectively (Fig. 8). Such percentages of mantle contribution refer to a MORB-like mantle. Indeed, fluid inclusions in olivine crystals of recent (<0.61 Ma) volcanic rocks of this region display R/R_A values in the range 7.29 – 8.03 confirming that the mantle source of these lavas did not suffer any important process of crustal contamination (Italiano et al., 2017). Such an important mantle contribution shows that the studied tectonic system acts as a permeable route for the upflow of fluids directly from the mantle.

5.1.6. Radon

The measured radon levels in the soils along the studied tectonic structure can be considered quite low (max 5.6 and median value 0.87 kBq m^{-3}), especially when compared with previous studies conducted along active fault zones, where much higher soil radon concentrations have been reported. Close to the Manisa Fault, values exceeding 35 kBq m^{-3} have been observed (Taşköprü et al., 2023), while studies from the İzmir Fault have reported concentrations up to 22 kBq m^{-3} (Masruoğlu et al., 2023; İçhedef et al., 2025). For comparison Yüce et al. (2017) in soil gases of the close by Amik basin found higher values (max 83.9 and median value 7.3 kBq m^{-3}), while Ciotoli et al. (2014) reports median soil ^{222}Rn values for 11 different intermontane plains in central Italy ranging from 6.47 to 58.8 kBq m^{-3}. These findings suggest that the studied region exhibits notably lower radon activity, which may be due to differences in geological structure, fault permeability, or soil characteristics. One of the factors that could explain these lower values is the lithology of the study area. Yüce et al. (2017) indeed observed a slight difference of Rn concentration in different rock units. The study area actually comprises lithologies with low concentrations of U which is the

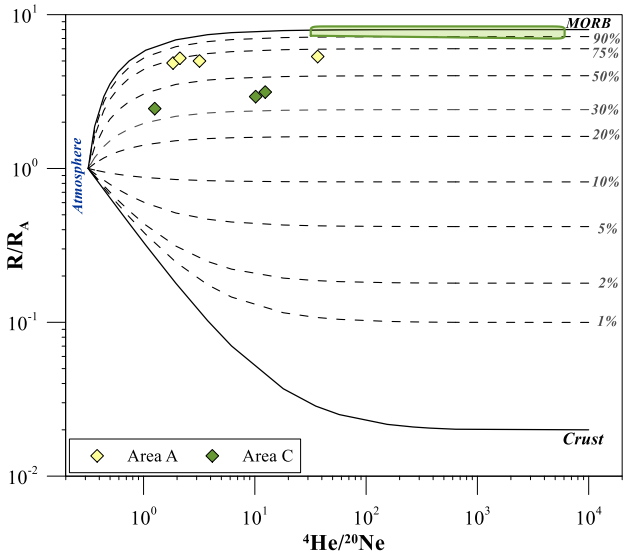

Fig. 8. R/R_A ratio vs. $^4He/^{20}Ne$ ratio binary plot. The dashed lines represent the mixing between atmosphere ($1R_A$, Ozima and Podosek, 2002; $^4He/^{20}Ne = 0.318$, Sano and Wakita, 1985), crust (0.01-0.02R_A, Ballentine and Burnard, 2002; $^4He/^{20}Ne > 1000$, Sano and Wakita, 1985) and MORB-type mantle (8 ± 1 R_A, Ozima and Podosek, 2002; $^4He/^{20}Ne > 1000$, Sano and Wakita, 1985) helium sources. The green area represents the R/R_A and $^4He/^{20}Ne$ data from fluid inclusions hosted in olivine phenocrystals from the nearby Amik and Toprakkale volcanic areas (Italiano et al., 2017).

precursor of the emitted ^{222}Rn. Mafic and ultramafic rocks, which compose prevailingly the ophiolitic sequence whose outcrops are widespread in the area, show generally U contents below 0.1 μg g^{-1} with the few values above referring to more evolved products (Dilek and Thy, 1998). The recent volcanic rocks outcropping in the area show also values mostly below 1 μg g^{-1} (Italiano et al., 2017). No data have been found for the remaining lithologies of the area but these are mostly sedimentary rocks which have U content generally lower than the average upper continental crust (2.5 – 2.8 μg g^{-1}; Reimann and De Caritat, 1998).

In area A, CO_2 is observed as the dominant gas component in the soil gas composition. Radon and CO_2 are generally expected to migrate together due to similar transport mechanisms in the subsurface environment. However, a negative correlation (−0.29) between radon and CO_2 was found, suggesting that the presence of high CO_2 concentrations may be influencing radon transport dynamics (Fig. 9). One possible explanation for this is that high CO_2 fluxes may dilute other soil gases, including radon. Additionally, a strong negative correlation (−0.62) between CO_2 and O_2 was observed, indicating that as CO_2 levels increase, O_2 levels significantly decrease (Fig. 9). This inverse relationship further supports the notion that deep-derived CO_2 plays a dominant role in the soil gas environment of this area, potentially displacing or diluting gases of shallow origin. Consequently, the observed correlations suggest that elevated CO_2 concentrations may lead to a reduction in both radon and O_2 levels.

5.2. CO_2 output estimation

In area B, CO_2 from almost all the samples can be attributed to an organic source. Only two sites may be ascribed to a mixed organic/deep source on statistical basis but the isotope composition indicates a purely organic origin ($\delta^{13}C$–$CO_2 < -21.7$ ‰). The contribution of this area to the geogenic degassing of the Osmaniye tectonic structure can therefore be considered negligible.

In the case of area A, instead, the probability plot of Fig. 5 evidenced three populations. Population III is characterized by a much higher mean CO_2 flux value (8513 g m^{-2} d^{-1}) and should be considered to represent the deep CO_2 degassing. Population I is characterized also in this area by low mean CO_2 flux value (11.9 g m^{-2} d^{-1}) and may represent the biological CO_2 background flux for the region. The mean CO_2 flux of population I is in line with CO_2 fluxes generally produced by the biological activity for different ecosystems (mean CO_2 fluxes from 0.2 to 21 g m^{-2} d^{-1}, Viveiros et al., 2010; Cardellini et al., 2017 and references therein) and with the biological background generally found in hydrothermal sites (Chiodini et al., 2008 and references therein). Population II, with intermediate flux values (mean value 389 g m^{-2} d^{-1}), represents a mixture of the two sources (deep degassing and shallow organic activity).

The obtained CO_2 flux map (Fig. 10) evidences two strongly anomalous areas which correspond to the areas with greatest soil and rock

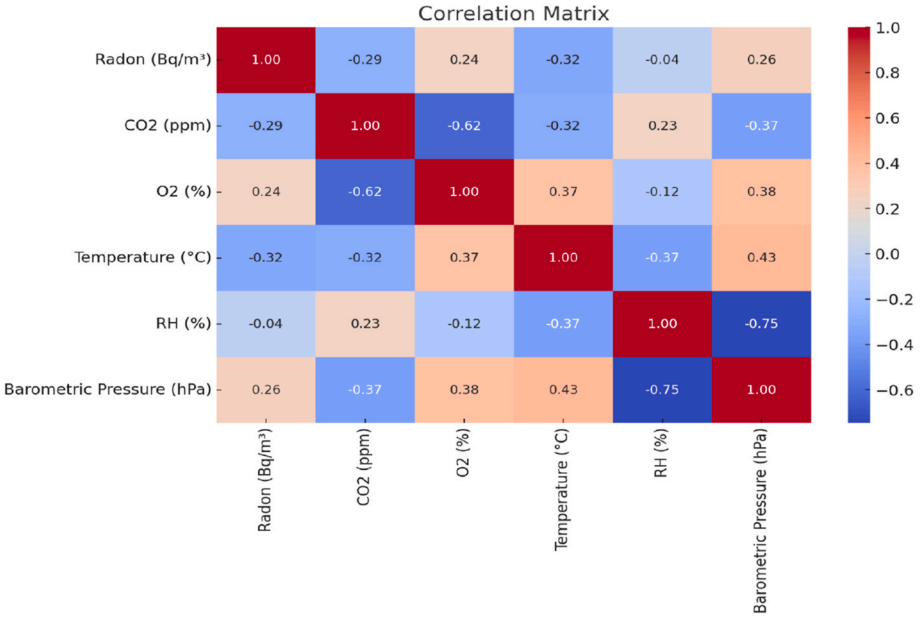

Fig. 9. Correlation matrix (Correlogram) showing the relationships between radon concentration and meteorological parameters taking into account both areas A and B. RH = relative humidity.

alteration. These two strongly degassing areas seem to be roughly parallel to the main direction of the Osmaniye segment on the EAFZ (Fig. 2). This may suggest that the structure that allows the upflow of abundant geogenic CO_2 in this area is one of the splay faults parallel to the main structure. Other areas with somewhat less pronounced degassing (intermediate colours in Fig. 10) but still clearly anomalous are generally related to areas with stunted or absent vegetation but with no apparent soil or rock alteration. Such areas seem not to follow the direction of the main structure.

One simple method to obtain an estimation of the total output of CO_2 from the investigated area is to multiply the mean flux value of each population obtained from the probability plot analysis by the surface area corresponding to the percentage of that population. For area A this results in a total CO_2 output of 65.2 t d^{-1} (Table 1). The contribution of population I, which is ascribable to almost exclusive organic origin, can be considered negligible (0.13 t d^{-1}).

Another method, considered more accurate (Lewicki et al., 2005), is the use of the sGs method (Cardellini et al., 2003). The total amount of released CO_2 estimated with such method is 54.3 ± 10 t d^{-1} over an area of 35,900 m^2. Such output is almost totally ascribable to deep geogenic sources with the contribution of biogenic CO_2 being at most 0.43 t d^{-1}) considering a biogenic CO_2 flux of 11.9 g m^{-2} d^{-1} (i.e., the mean CO_2 flux of population I) over the entire area.

The results of the two methods are quite similar but in the following of the discussion we will consider the second one which is considered at present the gold standard for CO_2 output estimations (Cardellini et al., 2003; Lewicki et al., 2005).

The estimated output is comparable to a volcanic system classified by Fischer et al. (2019) among the weak CO_2 emitters in their hydrothermal stage. Based on statistical calculations, the authors obtained a mean CO_2 output of 36 t d^{-1} from such kind of volcanic systems (Fischer et al., 2019). Such value is close to the estimated output of area A, suggesting that this area could be fed by a hydrothermal system. At the moment, excluding the occurrence of gases of possible hydrothermal origin (H_2 and CH_4), we have no further evidence of a geothermal reservoir. Furthermore, a similar CO_2 output (67 ± 7 t d^{-1}) has been documented also along an active tectonic system where both hydrothermal activity and magmatic intrusion have been definitely excluded (Li Vigni et al., 2022) underscoring the fact that such output does not necessarily need a heat source.

Although no CO_2 flux measurements have been performed in area C, the occurrence of significant deep CO_2 release to the atmosphere in this area is unlikely. The presence here of a hyperalkaline spring, points to a deep circulation along a fault zone within the ophiolitic sequence. The significant mantle contribution for He in the bubbling gases testifies for an injection of mantle fluids at the base of the fault. During upflow, when these fluids reach the hyperalkaline aquifer, He and CO_2 will be decoupled due to their very different chemical reactivity. The former, being inert, will continue undisturbed its travel to the Earth's surface. On the contrary, the latter would be lost either being precipitated as carbonate minerals due to the very high pH or, in the presence of the necessary conditions (occurrence of H_2 and metal catalysts), transformed in alkanes by Fischer-Tropsch-type reactions (Etiope and Sherwood Lollar, 2013).

5.3. *Relationships between geogenic degassing and the geodynamic context of the area*

Regional tectonic structures have long been recognised as geogenic degassing hotspots of the Earth's surface (Barnes et al., 1978; Irwin and Barnes, 1980; Tamburello et al., 2018). This is particularly true for extensional or/and transcurrent faults systems. The study area is mainly

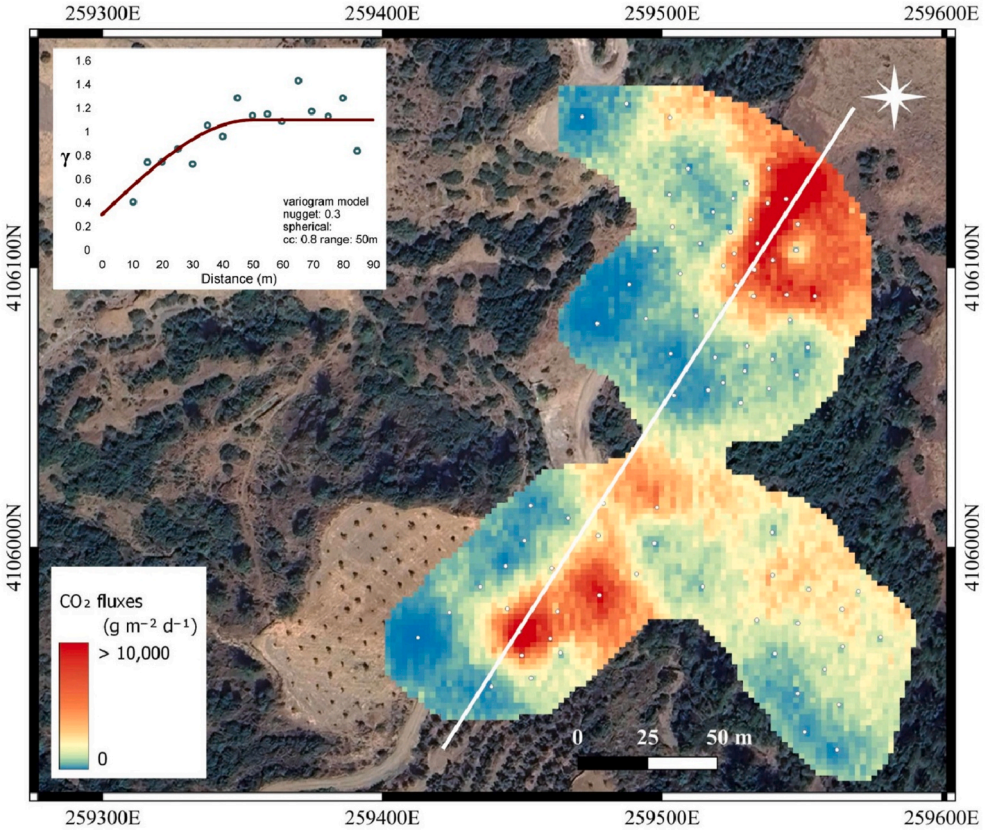

Fig. 10. CO_2 flux map of area A and associated variogram diagram. The map reports at each point the average of the CO_2 flux computed based on 100 simulations. The white line is the inferred diffuse degassing structure which follow the directions of the Osmaniye fault (Fig. 2) and other tectonic lineaments of the area (Emre et al., 2018). Map coordinates are expressed in meters (WGS84 UTM 37 N). Basemap from ESRI.

controlled by the Osmaniye segment of the EAFZ, which is a large-scale continental transform fault and constitutes the plate boundary between Arabian-African plates to the south and Anatolian Microplate to the north (Okay and Tüysüz, 1999). This deep-seated fault has also been suggested by many studies as the pathway for the extensive mantle-sourced young basaltic volcanism of the area (Polat et al., 1997; Yurtmen et al., 2000; Nikogosian et al., 2018). The same source justifies also the high proportion (>70%) of mantle contribution to the He measured in the gases released in the study area released through structures related to EAFZ.

Such a strong contribution of mantle-derived He is likely also favoured by the extensional regime of the area which brought to a substantial thinning of the crust. Previous studies (Vanacore et al., 2013; Bilim et al., 2016) indicate for the Osmaniye area a depth of the Moho at less than 30 km with the crust further thinning in the SW direction along the EAFZ. Simão et al. (2016) attributed extensional deformation and crustal thinning of the south-central part of Türkiye to its counter-clockwise rotation. This resulted in the upwelling of warmer upper mantle observed in tomographic studies (Simão et al., 2016). Such upwelling may explain the typical MORB-like He isotope imprint found by Italiano et al. (2017) in the fluid inclusions of olivine and pyroxenes of the recent basaltic rocks of the area and thinning of the crust justifies the lowest crustal contamination found in the fluids collected here with respect to those of the surrounding areas.

Such geodynamic regime (extension and crustal thinning) may favour also the degassing of geogenic CO_2 with mantle or deep crustal origin. While area A represent a very strong degassing hotspot along the Osmaniye fault evidencing CO_2 fluxes as high as 57,200 g m^{-2} d^{-1} and specific outputs of about 1500 t km^{-2} d^{-1}, other zones in the region may be also subject to geogenic degassing. Indeed, in the nearby Amik basin, a similar tectonic regime creates conditions favourable to CO_2 degassing (Yüce et al., 2017, 2026).

On the contrary, the structure of the shallowest part of the crust may be the reason why geogenic CO_2 degassing for area B is not measurable and for area C, though not measured, is highly improbable. For both areas the presence of ophiolitic rocks is probably the cause of removal of CO_2 from ascending fluids through chemical reactions as specified in the previous paragraph, but the presence of impermeable sediments or self-sealing processes within the fault zone cannot be ruled out. The contrasting degassing behaviour observed can be largely explained by differences in the mechanical and lithological characteristics of the shallow stratigraphic units, which exert a first-order control on permeability structure and gas transport. In areas dominated by rigid–brittle lithologies, such as Mesozoic to Early Tertiary carbonates, ophiolitic units of the Kızıldağ complex, and locally fractured Quaternary basalts, deformation is preferentially accommodated by brittle faulting and fracturing. This favours the development of interconnected fracture networks and enhances vertical permeability, facilitating the upward migration of deep-derived gases, particularly along active faults and their intersections. In contrast, sectors characterized by mechanically weaker, plastic or low-permeability units, including marl- and shale-rich sequences, the Andırın mélange, and fine-grained Pliocene–Quaternary basin-fill deposits, tend to inhibit focused gas ascent. In such settings, higher sealing capacity and more distributed deformation limit gas transport, resulting in subdued or negligible surface degassing. These lithological and mechanical contrasts provide a coherent framework for interpreting the observed spatial variability in degassing intensity across the study area.

Finally, with the presently available data it is not possible to assess the presence of an active hydrothermal system in the study area. The only clues are the strong alteration of rocks and soils in the zones of highest CO_2 flux from the soil and the composition of the collected gases in which hydrothermal species have been measured (H_2 and CH_4) or are presumed (H_2S). Such deep alteration could be due to oxidation of H_2S within the shallow part of the soil producing strongly reactive sulfuric acid (H_2SO_4), justifying the presence of sulfur and sulfate incrustations and efflorescences (see pictures in supplementary material). The presence in the area of an anomalous geothermal gradient (up to 80 °C/km - Bilim et al., 2017) may sustain small hydrothermal systems due to the deep circulation of meteoric water within the active tectonic structures of the area. The same tectonic structures have sometimes acted as preferential pathway for magmas as testified by the widespread outcrops of recent mafic volcanic rocks in the area (Italiano et al., 2017; Nikogosian et al., 2018). A basaltic dike that did not reach the surface may act as the heat source of a small scale, short living hydrothermal system.

Of course, alternative origins for the presence of the “hydrothermal” gases are, with the present data, equally probable. Hydrogen and CH_4 may be produced by alteration processes within the ophiolite sequence and the strong soil alteration may be due to H_2SO_4 deriving from oxidation of sulfides that can be found within the sediments instead of H_2S. The presence of a hydrothermal system below area A remains therefore an unconfirmed hypothesis.

6. Conclusions

The three investigated areas along the active segment of the EAFZ, despite being close to each other, show strongly contrasting degassing behaviours. The differences can be recognised both in terms of intensive (chemical and isotope composition of the gases) and extensive (CO_2 output) characteristics of the emitted fluids. Gas chemistry shows CO_2-dominated, N_2-dominated and CH_4-dominated compositions for areas A, B and C respectively. Isotope composition of He and C point to a strong mantle contribution (70 % of MORB-type mantle) and a deep geogenic CO_2 origin ($\delta^{13}C$–$CO_2 \sim 0‰$) for area A, a shallow organic origin of CO_2 ($\delta^{13}C$–$CO_2 \sim -22‰$) for area B and a likely abiotic origin of CH_4 ($\delta^{13}C$–$CH_4 \sim -8‰$) and a significant mantle contribution for He (40 % of MORB-type mantle) for area C. Moreover, area A is the site of an intense geogenic degassing with CO_2 soil fluxes sometimes exceeding 10^4 g m^{-2} d^{-1} totalling a yearly release of about 20,000 t of deep geogenic CO_2, while area B show almost exclusively low CO_2 soil fluxes (0.4 - 57 g m^{-2} d^{-1}) typical of shallow biologic activity within the soil and a negligible output of organic CO_2. No CO_2 soil flux measurements were made in area C, but the very low flux of bubbling gases, almost devoid of CO_2, makes a significant CO_2 output in this area very unlikely.

These big differences in degassing behaviour of the three areas may be attributed to many causes mainly connected to the geology of the shallowest part of the stratigraphic sequence. Fluids interacting with different lithologies may consume and/or produce certain gas species. The presence of rigid and brittle lithologies or intersections of tectonic structures may increase the permeability to deep derived gases allowing higher gas emissions at the surface in areas subject to tectonic stress. On the contrary, plastic and impermeable lithologies can hinder an easy ascent of gases almost reducing to zero their release to the atmosphere.

Finally, it should be underscored that the Osmaniye segment of the EAFZ was not involved in the destructive earthquakes of February 2023. The consequent stress release from these earthquakes may have highly increased the probability of the Osmaniye area to be site of intense seismic activity in the next years. Therefore, it would be essential to study possible precursory signal in the fluids emitted along this active structure. In particular, area A would be an important site for geochemical (H_2, CO_2, ^{222}Rn, CO_2-flux) permanently monitoring stations and discrete gas sampling. Parameters that should be measured at hourly (or at least daily) basis are H_2 and CO_2 concentrations and ^{222}Rn activity at 50 cm depth in the soil and CO_2-flux at the soil surface. Meteorological parameters should be contemporaneously acquired to filter possible interferences. Periodic (monthly – half-yearly) collection of gas samples for their chemical and isotope analysis in the laboratory should also be implemented including the bubbling gases of area C.

Funding

This research has been funded by the TUBITAK project 123Y301 and

by the Scientific Research Projects Coordination Unit of Hacettepe University under grant number 21551. Travel expenses of Walter D'Alessandro have been covered by INGV.

CRediT authorship contribution statement

G. Yüce: Conceptualization, Funding acquisition, Investigation, Methodology, Project administration, Resources, Supervision, Writing – original draft. **W. D'Alessandro:** Conceptualization, Data curation, Formal analysis, Investigation, Methodology, Resources, Validation, Visualization, Writing – original draft. **C.C. Fu:** Conceptualization, Investigation, Methodology, Resources, Writing – review & editing. **F. Italiano:** Conceptualization, Investigation, Writing – review & editing. **M. İçhedef:** Conceptualization, Data curation, Formal analysis, Investigation, Resources, Validation, Writing – original draft. **H. Elmacı:** Investigation, Writing – review & editing. **B. Kürkcüoğlu:** Investigation, Project administration, Writing – review & editing. **B. Kahraman:** Investigation, Project administration, Supervision, Writing – review & editing. **A. Demirtaş:** Investigation, Writing – review & editing. **L.H. Lin:** Resources, Validation, Writing – review & editing. **D. Yasin:** Investigation, Writing – review & editing. **Ş. Gürboğa:** Investigation, Visualization, Writing – review & editing. **A. Özdemir:** Investigation, Writing – review & editing. **L. Li Vigni:** Data curation, Formal analysis, Validation, Visualization, Writing – review & editing. **M. Tantillo:** Validation, Writing – review & editing. **H. Akıllı:** Investigation, Writing – review & editing. **A. Çiçek:** Investigation, Writing – review & editing. **L. Taşkıran:** Investigation, Writing – review & editing. **M. Toklu:** Investigation, Writing – review & editing. **S. Över:** Writing – review & editing. **T. Kılıç:** Writing – review & editing.

Declaration of competing interest

The authors declare that they have no known competing financial interests or personal relationships that could have appeared to influence the work reported in this paper.

Appendix A. Supplementary data

Supplementary data to this article can be found online at https://doi.org/10.1016/j.apgeochem.2026.106766.

Data availability

All data presented in this work have been included as supplementary materials in 2 Tables that comprise all analytical result of the collected gas samples (Table S1) and the soil CO_2 fluxes measured in the area including geographic coordinates (Table S2).

References

Akar, F., 2024. Spatio-temporal changes in b-value associated with the 2023 Türkiye earthquake. J. Earth Syst. Sci. 133, 185. https://doi.org/10.1007/s12040-024-02398-w.

Akinci, A., Dindar, A.A., Bal, I.E., Ertuncay, D., Smyrou, E., Cheloni, D., 2025. Characteristics of strong ground motions and structural damage patterns from the February 6th, 2023 Kahramanmaraş earthquakes, Türkiye. Nat. Haz. 121, 1209–1239.

Arger, J., Mitchell, J., Wateway, R.W.C., 2000. Neogene and Quaternary volcanism of SE Turkey. In: Bozkurt, E., Winchester, J.A., Piper, J.D.A. (Eds.), Tectonics and Magmatism in Turkey and the Surrounding Area, vol.173. Geological Society, London, Special Publications, pp. 459–487.

Şaroğlu, F., 1985. Doğu Anadolu'Nun Neotektonik Dönemde Jeolojik ve Yapısal Evrimi: İstanbul Üniversitesi. Fen Bilimleri Enstitüsü. PhD theses. (in Turkish).

Bağcı, U., Parlak, O., Höck, V., 2005. Whole rock and mineral chemistry of cumulates from the kızıldağ (hatay) ophiolite (turkey): clues for multiple magma generation during crustal accretion in the southern Neotethyan ocean. Mineral. Mag. 69, 39–62.

Ballentine, C.J., Burnard, P., 2002. Production, release and transport of noble gases in the continental crust. Rev. Mineral. Geochem. 47 (1), 481–538. https://doi.org/10.2138/rmg.2002.47.12.

Barbot, S., Luo, H., Wang, T., Hamiel, Y., Piatibratova, O., Javed, M.T., Braitenberg, C., Gurbuz, G., 2023. Slip distribution of the February 6, 2023 Mw 7.8 and Mw 7.6, Kahramanmaraş, Turkey earthquake sequence in the East Anatolian fault zone. Seismica 2 (3).

Barka, A., Kadinsky-Cade, K., 1988. Strike-slip fault geometry in Turkey and its influence on earthquake activity. Tectonics 7 (3), 663–684.

Barka, A., Reilinger, R., 1997. Active tectonics of the mediterranean region: deduced from GPS, neotectonic and seismicity data. Ann. Geofis. XI (3), 587–610.

Barnes, I., Irwin, W.P., White, D.E., 1978. Global distribution of carbon dioxide discharges and major zones of seismicity. US Geol. Surv. Wat. Resour. Division. https://doi.org/10.3133/wri7839.

Beyazpiriç, M., Usta, D., 2018. Türkiye Jeoloji Haritaları Serisi, Antakya-O36 Paftası. No. 267 in Turkish).

Bilgin, Z., Ercan, T., 1981. Ceyhan–osmaniye yöresindeki kuvaterner bazaltların petrolojisi. Turk. Jeol. Kurumu Bul. 24, 22–30 (in Turkish).

Bilim, F., Aydemir, A., Ates, A., 2016. Crustal thickness variations in the eastern mediterranean and southern Aegean region. Mar. Petrol. Geol. 77, 190–197.

Bilim, F., Aydemir, A., Ates, A., 2017. Tectonics and thermal structure in the gulf of iskenderun (southern Turkey) from the aeromagnetic, borehole and seismic data. Geothermics 70, 206–221.

Brune, S., Williams, S., Müller, D., 2017. Potential links between Continental rifting, CO_2 degassing and climate change through time. Nat. Geosci. 10, 941–947. https://doi.org/10.1038/s41561-017-0003-6.

Burton, M.R., Sawyer, G.M., Granieri, D., 2013. Deep carbon emissions from volcanoes. In: Hazen, R.M., Jones, A.P., Baross, J.A. (Eds.), Carbon in Earth. Rev. Mineral. Geochem. 75, 323–354. https://doi.org/10.2138/rmg.2013.75.11.

Burton-Ferguson, R., Aksu, A.E., Calon, T.J., Hall, J., 2005. Seismic stratigraphy and structural evolution of the Adana basin, eastern mediterranean. Mar. Geol. 221 (1-4), 189–222.

Camarda, M., De Gregorio, S., Favara, R., Gurrieri, S., 2007. Evaluation of carbon isotope fractionation of soil CO_2 under an advective–diffusive regimen: a tool for computing the isotopic composition of unfractionated deep source. Geochim. Cosmochim. Acta 71, 3016–3027.

Caracausi, A., Buttita, D., Picozzi, M., Paternoster, M., Stabile, T.A., 2022. Earthquakes control the impulsive nature of crustal helium degassing to the atmosphere. Nat. Comm. Earth & Envir 3, 224. https://doi.org/10.1038/s43247-022-00549-9.

Cardellini, C., Chiodini, G., Frondini, F., 2003. Application of stochastic simulation to CO_2 flux frim soil: mapping and quantification of gas release. J. Geophys. Res. 108, 2425.

Cardellini, C., Chiodini, G., Frondini, F., Avino, R., Bagnato, E., Caliro, S., Lelli, M., Rosiello, A., 2017. Monitoring diffuse volcanic degassing during volcanic unrest: the case of campi flegrei (italy). Sci. Rep. 7, 6757.

Chiodini, G., 2009. CO_2/CH_4 ratio in fumaroles a powerful tool to detect magma degassing episodes at quiescent volcanoes. Geophys. Res. Lett. 36, L02302. https://doi.org/10.1029/2008GL036347.

Chiodini, G., Caliro, S., Cardellini, C., Avino, R., Granieri, D., Schmidt, A., 2008. Carbon isotopic composition of soil CO_2 efflux, a powerful method to discriminate different sources feeding soil CO_2 degassing in volcanic-hydrothermal areas. Earth Planet Sci. Lett. 274, 372–379. https://doi.org/10.1016/j.epsl.2008.07.051.

Chiodini, G., Caliro, S., Cardellini, C., Frondini, F., Inguaggiato, S., Matteucci, F., 2011. Geochemical evidence for and characterization of CO_2 rich gas sources in the epicentral area of the Abruzzo 2009 earthquakes. Earth Planet Sci. Lett. 304, 389–398.

Chiodini, G., Cardellini, C., Di Luccio, F., Selva, J., Frondini, F., Caliro, S., Rosiello, A., Beddini, G., Ventura, G., 2020. Correlation between tectonic CO_2 Earth degassing and seismicity is revealed by a 10-year record in the apennines, Italy. Sci. Adv. 6, eabc2938.

Chiodini, G., Cioni, R., Guidi, M., Raco, B., Marini, L., 1998. Soil CO_2 flux measurements in volcanic and geothermal areas. Appl. Geochem. 13 (5), 543–552. https://doi.org/10.1016/S0883-2927(97)00076-0.

Ciotoli, G., Bigi, S., Tartarello, C., Sacco, P., Lombardi, S., Ascione, A., Mazzoli, S., 2014. Soil gas distribution in the main coseismic surface Rupture Zone of the 1980, Ms = 6.9, Irpinia Earthquake (Southern Italy). J. Geophys. Res. Solid Earth 119, 2440–2461. https://doi.org/10.1002/2013JB010508.

D'Alessandro, W., Li Vigni, L., Gagliano, A.L., Calabrese, S., Kyriakopoulos, K., Daskalopoulou, K., 2020. CO_2 release to the atmosphere from thermal springs of sperchios Basin and northern Euboea (Greece). The contribution of "hidden" degassing. Appl. Geochem. 119, 104660. https://doi.org/10.1016/j.apgeochem.2020.104660.

D'Alessandro, W., Yüce, G., Italiano, F., Bellomo, S., Gülbay, A.H., Yasin, D.U., Gagliano, A.L., 2018. Large compositional differences in the gases released from the Kizildag ophiolitic body (Turkey): evidences of prevailingly abiogenic origin. Mar. Petrol. Geol. 89, 174–184. https://doi.org/10.1016/j.marpetgeo.2016.12.017.

Daskalopoulou, K., Calabrese, S., Gagliano, A.L., D'Alessandro, W., 2019. Estimation of the geogenic carbon degassing of Greece. (Greece). Appl. Geochem. 106, 60–74.

David, M., 1977. Geostatistical ore reserve estimation. Developments in Geomathematics 2. Elsevier, Amsterdam, p. 364.

Deutsch, C.V., Journel, A.G., 1998. GSLIB: Geostatistical Software Library and User's Guide, second ed. Oxford University Press, New York.

Dewey, J.F., Hempton, M.R., Kidd, W.S.F., Saroğlu, F.A.M.C., Şengör, A.M.C., 1986. Shortening of continental lithosphere: the neotectonics of Eastern Anatolia—A young collision zone. Geol. Soc. London Spec. Publ. 19 (1), 1–36.

Dilek, Y., Thy, P., 1998. Structure, petrology and seafloor spreading tectonics of the Kizildag ophiolite, Turkey. In: Mills, R.A., Harrison, K. (Eds.), Modern Ocean Floor Processes and the Geological Record, vol. 148. Geol. Soc. London Spec. Publ., pp. 43–69

Dilek, Y., Thy, P., 2009. Island arc tholeiite to boninitic melt evolution of the Cretaceous Kızıldağ (Turkey) ophiolite: model for multi-stage early arc–forearc magmatism in Tethyan subduction factories. Lithos 113, 68–87.

Du, J., Cheng, W., Zhang, Y., Jian, C., Guan, Z., 2006. Helium and Carbon isotopic compositions of thermal springs in earthquake zone of Sichuan, Southwestern China. J. Asian Earth Sci. 26, 533–539. https://doi.org/10.1016/j.jseaes.2004.11.006.

Duman, T.Y., Emre, Ö., 2013. The East Anatolian Fault: geometry, segmentation, and jog characteristics. Geol. Soc. London Spec. Publ. 372, 495–529. https://doi.org/10.1144/SP372.14.

Elmacı, H., Kürçer, A., Özdemir, E., Avcı, H.O., Güven, C., Aydoğan, H., Güler, T., Avcu, İ., Olgun, Ş., Yüce, A.A., Özalp, S., 2024. Bölüm 2: 06 şubat 2023 pazarcık (kahramanmaraş) depremi yüzey kırığı. 06 Şubat 2023 Kahramanmaraş Deprem Yüzey Kırıkları Kitabı. Maden Tetkik ve Arama Genel Müdürlüğü Özel Yayın Serisi, MTA, Ankara (in Turkish).

Emre, Ö., Duman, T.Y., Özalp, S., Şaroğlu, F., Olgun, Ş., Elmacı, H., Çan, T., 2018. Active fault database of Turkey. Bull. Earthquake Eng. 16 (8), 3229–3275. https://doi.org/10.1007/s10518-016-0041-2.

Şengör, A., Özeren, S., Genç, T., Zor, E., 2003. East Anatolian high plateau as a mantle supported, north-south shortened domal structure. Geophys. Res. Lett. 30 (24). https://doi.org/10.1029/2003GL017858.

Şengör, A.M.C., Görür, N., Şaroğlu, F., 1985. Strike-Slip Faulting and Basin Related Formation in Zones of Tectonic Escape, vol. 37. SEPM Spec. Publ., pp. 227–440

Etiope, G., Schoell, M., Hosgörmez, H., 2011. Abiotic methane flux from the chimaera seep and tekirova ophiolites (turkey): understanding gas exhalation from low temperature serpentinization and implications for Mars. Earth Planet Sci. Lett. 310, 96–104. https://doi.org/10.1016/j.epsl.2011.08.001.

Etiope, G., Ionescu, A., 2015. Low-temperature catalytic CO_2 hydrogenation with geological quantities of ruthenium: a possible abiotic CH_4 source in chromite-rich serpentinized rocks. Geofluids 15, 438–452. https://doi.org/10.1111/gfl.12106.

Etiope, G., Sherwood Lollar, B., 2013. Abiotic methane on Earth. Rev. Geophys. 51, 276–299. https://doi.org/10.1002/rog.20011.

Fiebig, J., Stefánsson, A., Ricci, A., Tassi, F., Viveiros, F., Silva, C., Lopez, T.M., Schreiber, C., Hofmann, S., Mountain, B.W., 2019. Abiogenesis not required to explain the origin of volcanic-hydrothermal hydrocarbons. Geochem. Persp. Lett. 11, 23–27.

Fiebig, J., Tassi, F., D'Alessandro, W., Vaselli, O., Woodland, A.B., 2013. Carbon-bearing gas geothermometers for volcanic–hydrothermal systems. Chem. Geol. 351, 66–75.

Fischer, T.P., Arellano, S., Carn, S., Aiuppa, A., Galle, B., Allard, P., Lopez, T., Shinohara, H., Kelly, P., Werner, C., Cardellini, C., Chiodini, G., 2019. The emissions of CO_2 and other volatiles from the world's subaerial volcanoes. Sci. Rep. 9, 18716. https://doi.org/10.1038/s41598-019-54682-1.

Fu, C.C., Yang, T.F., Chen, C.H., Lee, L.C., Wu, Y.M., Liu, T.K., Walia, V., Kumar, A., Lai, T.H., 2017. Spatial and temporal anomalies of soil gas in northern Taiwan and its tectonic and seismic implications. J. Asian Earth Sci. 149, 64–77. https://doi.org/10.1016/j.jseaes.2017.02.032.

Fu, C.C., Yang, T.F., Walia, V., Liu, T.K., Lin, S.J., Chen, C.H., Hou, C.S., 2009. Variations of soil-gas composition around the active chihshang Fault in a plate suture zone, eastern Taiwan. Radiat. Meas. 44, 940–944. https://doi.org/10.1016/j.radmeas.2009.10.095.

Gökçeoğlu, C., 2023. 2023 Kahramanmaraş – türkiye earthquakes: a general overview, 6 February Int. Arch. Photogramm. Remote Sens. Spatial Inf. Sci. XLVIII-M-1–2023, 417–424. https://doi.org/10.5194/isprs-archives-XLVIII-M-1-2023-417-2023, 2023.

Gürboğa, Ş., Kayadibi, Ö., Akilli, H., Arikan, S., Tan, S., 2024. Preliminary results of the great Kahramanmaraş 6 February 2023 earthquakes (MW 7.7 and 7.6) and 20 February 2023 Antakya earthquake (MW 6.4), eastern Türkiye. Turk. J. Earth Sci. 33 (1), 22–39.

Hempton, M.R., 1987. Constraints on Arabian plate motion and extensional history of the Red Sea. Tectonics 6, 687–705.

Hirose, T., Kawagucci, S., Suzuki, K., 2011. Mechanoradical H_2 generation during simulated faulting: implications for an earthquake-driven subsurface biosphere. Geophys. Res. Lett. 38, L17303. https://doi.org/10.1029/2011.gl048850.

Hu, J., Liu, M., Taymaz, T., Ding, L., Irmak, T.S., 2025. Characteristics of strong ground motion from the 2023 Mw 7.8 and Mw 7.6 Kahramanmaraş earthquake sequence. Bull. Earthquake Eng. 23, 1225–1254.

İçhedef, M., Sapmaz, İ., Taşköprü, C., Walia, V., 2025. Analysing temporal variations in Radon concentrations: identifying trends and changes. Terra Nova 37 (4), 263–274. https://doi.org/10.1111/ter.12774.

Şimşek, E., Parlak, O., Robertson, A.H., 2023. Ion-probe (SIMS) U-Pb geochronology and geochemistry of the Upper Cretaceous Kızıldağ (Hatay) ophiolite: implications for supra-subduction zone spreading in the Southern Neotethys. Geosystems and Geoenvironment 2 (3), 100165.

Irwin, W.P., Barnes, I., 1980. Tectonic relations of carbon dioxide discharges and earthquakes. J. Geophys. Res. 85 (B6), 3115–3121. https://doi.org/10.1029/JB085iB06p03115.

Italiano, F., Sasmaz, A., Yüce, G., Okan, O.O., 2013. Thermal fluids along the East Anatolian Fault Zone (EAFZ): geochemical features and relationships with the tectonic setting. Chem. Geol. 339, 103–114. https://doi.org/10.1016/j.chemgeo.2012.07.027.

Italiano, F., Yüce, G., Di Bella, M., Rojay, B., Sabatino, G., Tripodo, A., Martelli, M., Rizzo, A.L., Misseri, M., 2017. Noble gases and rock geochemistry of alkaline intraplate volcanics from the Amik and Ceyhan-Osmaniye areas, SE Turkey. Chem. Geol. 469, 34–46. https://doi.org/10.1016/j.chemgeo.2017.04.003.

Jia, Z., Jin, Z., Marchandon, M., Ulrich, T., Gabriel, A.A., Fan, W., Shearer, P., Zou, X., Rekoske, J., Bulut, F., Garagon, A., 2023. The complex dynamics of the 2023 Kahramanmaraş, Turkey, M w 7.8-7.7 earthquake doublet. Science 381 (6661), 985–990.

Karabacak, V., 2007. Quaternary Activity of the Northern Dead Sea Fault Zone. PhD thesis. Eskisehir Osmangazi University, Natural and Applied Sciences Institute [in Turkish with English abstract].

Karabacak, V., Akyüz, H.S., Kıyak, N.G., Altunel, E., Meghraoui, M., Yönlü, Ö., 2012. The late Quaternary activity of the east Anatolian Fault Zone between Gölbaşı (Adıyaman) and Karataş (Adana). TUBITAK (The Scientific & Technological Research Council of Turkey) Research Project. Final Report. Project No. 109Y043.

Karabacak, V., Özkaymak, Ç., Sözbilir, H., Tatar, O., Aktuğ, B., Özdağ, Ö.C., Çakir, R., Aksoy, E., Koçbulut, F., Softa, M., Akgün, E., Demir, A., Arslan, G., 2023. The 2023 Pazarcık (Kahramanmaraş, Türkiye) earthquake (Mw 7.7): implications for surface rupture dynamics along the East Anatolian Fault Zone. J. Geol. Soc. 180 (3). https://doi.org/10.1144/jgs2023-020 jgs2023-020.

Kerrick, D.M., 2001. Present and past nonanthropogenic CO_2 degassing from the solid earth. Rev. Geophys. 39, 565–585.

Kocaman, İ., 2023. The effect of the Kahramanmaraş earthquakes (Mw 7.7 and Mw 7.6) on historical masonry mosques and Minarets. Eng. Fail. Anal. 149, 107225.

Koçyiğit, A., Yılmaz, A., Adamia, S., Kuloshvili, S., 2001. Neotectonics of east Anatolian plateau (Turkey) and lesser caucasus: implication for transition from thrusting to strike-slip faulting. Geodin. Acta 14, 177–195. https://doi.org/10.1080/09853111.2001.11432443.

Kürçer, A., Elmacı, H., Özdemir, E., Güven, C., Güler, T., Avcu, İ., Olgun, Ş., Avcı, H.O., Aydoğan, H., Yüce, A.A., Çetin, F.E., Ayrancı, A., Akyol, Z., Soykasap, Ö.A., Altuntaş, G., Demirörs, U., Karayazı, O., Bayrak, A., Özalp, S., 2023. 06 Şubat Pazarcık (Kahramanmaraş) Depremi (Mw 7,8) Saha Gözlemleri ve Değerlendirmeler. MTA Genel Müdürlüğü, Rapor No: 14138, 198 s., Ankara (in Turkish).

Leong, J.A., Nielsen, M., McQueen, N., Karolyte, R., Hillegonds, D.J., Ballentine, C., Darrah, T., McGillis, W., Kelemen, P., 2023. H_2 and CH_4 outgassing rates in the Samail ophiolite, Oman: implications for low-temperature, continental serpentinization rates. Geochim. Cosmochim. Acta 347, 1–15.

Lewicki, J.L., Bergfeld, D., Cardellini, C., Chiodini, G., Granieri, D., Varley, N., Werner, C., 2005. Comparative soil CO_2 flux measurements and geostatistical estimation methods on Masaya volcano. Nicaragua. Bull. Volcanol. 68, 76–90. https://doi.org/10.1007/s00445-005-0423-9.

Li Vigni, L., Cardellini, C., Temovski, M., Ionescu, A., Molnár, K., Palcsu, L., Gagliano, A. L., Cappuzzo, S., D'Alessandro, W., 2022. Duvalo "Volcano" (North Macedonia): a purely tectonic-related CO_2 degassing system. Geochem. Geophys. Geosys. 23 (4). https://doi.org/10.1029/2021GC010198 e2021GC010198.

Li Vigni, L., Temovski, M., Cardellini, C., Molnár, K., Ionescu, A., Mirčovski, V., et al., 2025. Toward solving the mystery of elevated tectonic degassing in South Eastern Europe: insights from gas discharges along the Vardar suture (North Macedonia). Geochem. Geophys. Geosys. 26. https://doi.org/10.1029/2025GC012177 e2025GC012177.

Masruoğlu, G., Altun, C., Şentürk, M.Z., İçhedef, M., Taşköprü, C., 2023. Variation of soil gas $^{222}Rn/^{220}Rn$ concentration ratios along the Pınarbaşı segment of İzmir faupt. J. Radioanal. Nucl. Chem. 332, 4739–4743. https://doi.org/10.1007/s10967-023-08910-8.

Mayhew, L.E., Ellison, E.T., McCollom, T.M., Trainor, T.P., Templeton, A.S., 2013. Hydrogen generation from low-temperature water–rock reactions. Nat. Geosci. 6, 478–484. https://doi.org/10.1038/ngeo1825.

Meghraoui, M., Cakir, Z., Kariche, J., Toussaint, R., Provost, F., Karabacak, V., Sbeinati, R., Altunel, E., Nemer, T., 2025. The 2023 Mw 7.8 Kahramanmaraş earthquake rupture increases potential failure along the northern Dead sea Fault. Tectonophysics 910, 230799.

Melgar, D., Taymaz, T., Ganas, A., Crowell, B.W., Öcalan, T., Kahraman, M., Tsironi, V., Yolsal-Çevikbil, S., Valkaniotis, S., Irmak, T.S., Eken, T., 2023. Sub-and super-shear ruptures during the 2023 Mw 7.8 and Mw 7.6 earthquake doublet in SE Türkiye. Seismica 2 (3). https://doi.org/10.26443/seismica.v2i3.387.

Meng, J., Kusky, T., Mooney, W.D., Bozkurt, E., Bodur, M.N., Wang, L., 2024. Surface deformations of the 6 February 2023 earthquake sequence, eastern Türkiye. Science 383 (6680), 298–305.

Milkov, A.V., Etiope, G., 2018. Revised genetic diagrams for natural gases based on a global dataset of >20,000 samples. Org. Geochem. 125, 109–120.

Neubeck, A., Thanh Duc, N., Hellevang, H., Oze, C., Bastviken, D., Bacsik, Z., Holm, N.G., 2014. Olivine alteration and H_2 production in carbonate-rich, low temperature aqueous environments. Planet. Space Sci. 96, 51–61.

Nikogosian, I.K., Bracco Gartner, A.J.J., van Bergen, M.J., Mason, P.R.D., van Hinsbergen, D.J.J., 2018. Mantle sources of recent Anatolian intraplate magmatism: a regional plume or local tectonic origin? Tectonics 37, 4535–4566. https://doi.org/10.1029/2018TC005219.

Okay, A.I., Tüysüz, O., 1999. Tethyan sutures of northern Turkey. Geol. Soc. London Spec. Publ. 156 (1).

Ozima, M., Podosek, F.A., 2002. Noble Gas Geochemistry, second ed. Cambridge University Press, p. 286.

Polat, A., Kerrich, R., Casey, J.F., 1997. Geochemistry of Quaternary basalts erupted along the east Anatolian and Dead Sea fault zones of southern Turkey: implications for mantle sources. Lithos 40, 55–68.

Randazzo, P., Caracausi, A., Aiuppa, A., Cardellini, C., Chiodini, G., et al., 2021. Active degassing of deeply sourced fluids in central Europe: new evidences from a geochemical study in Serbia. Geochem. Geophys. Geosys. 22 (11). https://doi.org/10.1029/2021GC010017 e2021GC010017.

Reilinger, R., McClusky, S., Vernant, P., Lawrence, S., Ergintav, S., Cakmak, R., Ozener, H., Kadirov, F., Guliev, I., Stepanyan, R., Nadariya, M., 2006. GPS constraints on continental deformation in the Africa-Arabia-Eurasia continental collision zone and implications for the dynamics of plate interactions. J. Geophys. Res. 111 (B5), B05411. https://doi.org/10.1029/2005JB004051.

Reimann, C., de Caritat, P., 1998. Chemical Elements in the Environment: Factsheets for the Geochemist and Environmental Scientist. Springer-Verlag Berlin Heidelberg. https://doi.org/10.1007/978-3-642-72016-1.

Reitman, N.G., Briggs, R.W., Barnhart, W.D., Hatem, A.E., Thompson Jobe, J.A., DuRoss, C.B., Gold, R.D., Mejstrik, J.D., Collett, C., Koehler, R.D., Akçiz, S., 2023. Rapid surface rupture mapping from satellite data: the 2023 Kahramanmaraş, Turkey (Türkiye), earthquake sequence. Seism. Rec. 3 (4), 289–298.

Robertson, A., Unlügenç, Ü.C., İnan, N., Taşli, K., 2004. The Misis–andırın complex: a Mid-Tertiary melange related to late-stage subduction of the southern neotethys in S Turkey. J. Asian Earth Sci. 22 (5), 413–453.

Rosakis, A., Abdelmeguid, M., Elbanna, A., 2023. Evidence of early supershear transition in the Mw 7.8 Kahramanmaraş earthquake from near-field records. arXiv preprint arXiv:2302.07214.

Sano, Y., Marty, B., 1995. Origin of carbon in fumarolic gas from island arcs. Chem. Geol. 119, 265–274.

Sano, Y., Wakita, H., 1985. Geographical distribution of $^{3}He/^{4}He$ ratios in Japan: Implicatiois for arc tectonics and incipient magmatism. J. Geophys. Res. 90, 8729–8741. https://doi.org/10.1029/JB080i010p08729.

Sato, M., Sutton, A.J., McGee, K.A., Russell-Robinson, S., 1986. Monitoring of hydrogen along the san andreas and Calaveras faults in central California in 1980–1984. J. Geophys. Res. 91 (B12), 12315–12326. https://doi.org/10.1029/JB091iB12p12315.

Sengör, A.M.C., Yilmaz, Y., 1981. Tethyan evolution of Turkey: a plate tectonic approach. Tectonophysics 75, 181–241.

Sharma, V., Biswas, R., 2025. Seismic quiescence and b-value anomalies preceding the 6th February 2023 earthquake doublet (MW 7.8, MW 7.6) in Kahramanmaraş, Türkiye: a comprehensive analysis of seismic parameters along the East Anatolian Fault Zone. Acta Geophys. 73, 1159–1185.

Simão, N.M., Nalbant, S.S., Sunbul, F., Komec Mutlu, A., 2016. Central and eastern Anatolian crustal deformation rate and velocity fields derived from GPS and earthquake data. Earth Planet Sci. Lett. 433, 89–98.

Sinclair, A.J., 1974. Selection of threshold values in geochemical data using probability graphs. J. Geochem. Explor. 3, 129–149. https://doi.org/10.1016/0375-6742(74)90030-2.

Sümengen, M., 2014. Türkiye Jeoloji Haritaları Serisi, Gaziantep-N36 Paftası. No: 220 (in Turkish).

Sugisaki, R., Ido, M., Takeda, H., Isobe, Y., Hayashi, Y., Nakamura, N., Satake, H., Mizutani, Y., 1983. Origin of hydrogen and carbon dioxide in fault gases and its relation to fault activity. J. Geol. 91 (3), 239–258. https://doi.org/10.1086/628769.

Taşköprü, C., Içhedef, M., Oral, A.E., Saç, M.M., Sözbilir, H., 2023. The exchange of radon gas concentration along Manisa fault. J. Radioanal. Nucl. Chem. 332, 4721–4737. https://doi.org/10.1007/s10967-023-08934-0.

Tamburello, G., Pondrelli, S., Chiodini, G., Rouwet, D., 2018. Global-scale control of extensional tectonic of CO_2 earth degassing. Nat. Comm. 9, 4608.

Tanırlı, M., Rızaoğlu, T., 2016. Whole-rock and mineral chemistry of mafic cumulates from the low-Ti ophiolite in the southern part of Kahramanmaraş, Turkey. Russian Geol. Geophys. 57 (10), 1398–1418.

Toutain, J.P., Baubron, J.C., 1999. Gas geochemistry and seismotectonics: a review. Tectonophysics 304, 1–27.

Vanacore, E.A., Taymaz, T., Saygin, E., 2013. Moho structure of the Anatolian Plate from receiver function analysis. Geophys. J. Int. 193, 329–337.

Viveiros, F., Cardellini, C., Ferreira, T., Caliro, S., Chiodini, G., Silva, C., 2010. Soil CO_2 emissions at Furnas volcano, São Miguel Island, Azores archipelago: volcano monitoring perspectives, geomorphologic studies and land use planning application. J. Geophys. Res. 115, B12208.

Wells, D.L., Coppersmith, K.J., 1994. New empirical relationships among magnitude, rupture length, rupture width, rupture area, and surface displacement. Bull. Seismol. Soc. Am. 84 (4), 974–1002.

Williams, G.D., Ünlügenç, U.C., Kelling, G., Demirkol, C., 1995. Tectonic controls on stratigraphic evolution of the Adana Basin, Turkey. J. Geol. Soc. 152 (5), 873–882.

Yang, T.F., Lan, T.F., Lee, H.F., Fu, C.C., Chuang, P.C., Lo, C.H., Chen, C.H., Chen, C.T.A., Lee, C.S., 2005. Gas compositions and helium isotopic ratios of fluid samples around Kueishantao, NE offshore Taiwan and its tectonic implications. Geochem. J. 39, 469–480. https://doi.org/10.2343/geochemj.39.469.

Yüce, G., Fu, C.C., D'Alessandro, W., Gulbay, A.H., Lai, C.W., Bellomo, S., Yang, T.F., Italiano, F., Walia, V., 2017. Geochemical characteristics of soil radon and carbon dioxide within the Dead Sea Fault and Karasu Fault in the Amik Basin (Hatay). Turkey. Chem. Geol. 469, 129–146. https://doi.org/10.1016/j.chemgeo.2017.01.003.

Yüce, G., Fu, C.C., D'Alessandro, W., Kahraman, B., Kürkcüoglu, B., Italiano, F., Gulbay, A.H., Elmacı, H., İçhedef, M., Özdemir, A., Akıllı, H., Yasin, D., Gürboğa, Ş. D., Demirtaş, A., Lin, L.H., Wang, P.L., Över, S., 2026. Soil gas investigations in Hatay-Reyhanlı (Türkiye): implications for buried fault detection and seismic hazard assessment. Geochem. Geophys. Geosys. 27 (1). https://doi.org/10.1029/2025GC012419 e2025GC012419.

Yüce, G., Italiano, F., D'Alessandro, W., Yalcin, T.H., Yasin, D.U., Gulbay, A.H., Ozyurt, N.N., Rojay, B., Karabacak, V., Bellomo, S., Brusca, L., Yang, T., Fu, C.C., Lai, C.W., Ozacar, A., Walia, V., 2014. Origin and interactions of fluids circulating over the Amik Basin (Hatay-Turkey) and relationships with the hydrologic, geologic and tectonic settings. Chem. Geol. 388, 23–39. https://doi.org/10.1016/j.chemgeo.2014.09.006.

Yetiş, C., Kelling, G., Gökçen, S.L., Baroz, F., 1995. A revised stratigraphic framework for Late Cenozoic sequences in the northeastern Mediterranean region. Geol. Rundsch. 84, 794–812.

Yurtmen, S., Rowbotham, G., Işler, F., Floyd, P.A., 2000. Petrogenesis of basalts from southern Turkey: the Plio-Quaternary volcanism to the north of Iskenderun Gulf. Geol. Soc. London, Spec. Publ. 173 (1), 489–512. https://doi.org/10.1144/gsl.sp.2000.173.01.23.

Zhou, X., Yan, Y., Fang, W., Wang, W., Shi, H., Li, P., 2021. Short-Term seismic precursor anomalies of hydrogen concentration in Luojishan hot Spring bubbling gas, Eastern Tibetan Plateau. Front. Earth Sci. 8, 586279. https://doi.org/10.3389/feart.2020.586279.